HELIUM ISOTOPE OCEANOGRAPHY

HELIUM ISOTOPE OCEANOGRAPHY

By

MUDASSAR ALI BEG, B.Sc., M.Sc.

A Thesis

Submitted to the School of Graduate Studies

in Partial Fulfilment of the Requirements

for the Degree

Doctor of Philosophy

McMaster University

November 1971

DOCTOR OF PHILOSOPHY (1971) McMASTER UNIVERSITY
(Physics) Hamilton, Ontario.

TITLE: Helium Isotope Oceanography

AUTHOR: Mudassar Ali Beg, B.Sc. (University of Panjab, Pakistan)

M.Sc. (University of Sind)

SUPERVISOR: Professor W. B. Clarke

NUMBER OF PAGES: x, 118

ABSTRACT

Measurements of $^{3}He/^{4}He$ ratios have been carried out on gaseous samples extracted from Pacific and S. Atlantic deep waters using a high sensitivity mass spectrometer. Large enrichments, up to 34%, relative to the atmospheric $^{3}He/^{4}He$ ratio were found -- the Pacific values are about four times higher than the Atlantic values. Total helium and neon contents were also measured in the same samples by means of the isotope dilution technique. Saturation anomalies as high as 16 and 8% respectively for He and Ne were observed. The excesses

of ^{3}He, He and Ne show a definite trend with the depth, with a maximum at mid-depths (1.5 - 3 km). The relationship of the rare gas data to temperature-salinity profiles of the water masses involved is also discussed.

Assuming all the Ne excess to be of atmospheric origin, the ^{4}He excess has been corrected to obtain the non-atmospheric ^{4}He excess. It is found that about 60% of the Pacific and all the S. Atlantic ^{4}He excess is due to atmospheric origin. It is shown that the oceanic ^{3}He excess is explainable only if a source of ^{3}He is present in the oceans, as the existing possible production mechanisms of ^{3}He fail to account for the observed ^{3}He profiles. Since the ^{3}He excess shows a correlation with the non-atmospheric ^{4}He excess and the only possible source of radiogenic ^{4}He is solid earth, therefore, it is suggested that the ^{3}He excess in the oceans is of primordial origin leaking through the earth's crust. The average flux rate of primordial ^{3}He is estimated at 5.9 atoms cm^{-2} sec^{-1}.

ACKNOWLEDGEMENTS

It is a pleasure to express my sincere gratitude to Dr. W. B. Clarke who, besides guidance, has given unselfishly of his time and energy throughout the study and research leading to this thesis. I have greatly benefited from his many insights and from his stimulating and original approach to Physics. I would also like to thank Drs. C. C. McMullen, R. H. McNutt, T. J. Kennett and C. E. Rees for valuable suggestions.

This work would never have reached its present stage without the cooperation of Prof. H. Craig of Scripps Institution of Oceanography. He not only collected most of the samples but was just as interested in the outcome of the experiments as the author of this thesis. Thanks are also due to Prof. P. J. Wangersky of Dalhousie University who collected the South Atlantic samples. I am obliged to Messrs. G. Kugler, A. Teitsma, W. J. Jenkins and E. M. Beaver for their cooperation and assistance, and Mrs. Stella Smith for the difficult task of typing this manuscript.

I wish to extend sincere thanks to my parents for their patience, prayers and encouragement, and to my wife

who besides the above qualities also tolerated many discussions about this work.

This work was made possible through awards from the Commonwealth Scholarship by the Pakistan and Canadian Governments, and Teaching Assistantship by McMaster University.

TABLE OF CONTENTS

LIST OF TABLES

LIST OF ILLUSTRATIONS

GLOSSARY OF SYMBOLS USED

α = Isotopic fractionation factor for helium isotopes in water = $\frac{\beta(^3He)}{\beta(^4He)}$

β = Bunsen solubility coefficient for a gas.

C = Concentration of a gas in sea water in ml/kg at a given T and S.

C^* = Solubility of a gas in sea water in ml/kg at the same T and S.

$\delta(^3He)\%$ = Percent excess of $(^3He/^4He)_{sea}$ relative to $(^3He/^4He)_{air}$.

$\Delta\%$ = $[(C/C^*)-1] \times 100$ = Saturation anomaly of a gas.

$\Delta'(He)$ = Non-atmospheric component of $\Delta(He)$.

f = Measure of the air injection component in $\Delta(He)$ = $[\Delta(He) - \Delta'(He)]/\Delta(Ne)$.

p_o = Concentration of a gas in air

p = Partial pressure of a gas.

Φ_i = Flux of isotope i in atoms cm^{-2} sec^{-1}.

S‰ = Salinity of a water sample in per mil.

T(°C) = Potential temperature of a water sample.

CHAPTER I

INTRODUCTION

A. INTRODUCTION

The ocean is the largest single geographical feature of our planet. Its interaction with the atmosphere largely determines the global climate. Besides local upwelling and surface currents, there is the turnover cycle that takes several hundred years. These processes are essential for sustaining life and a more detailed understanding is of considerable importance.

Generally, the studies of dissolved gases in sea water have been initiated with one or more of the following objects.

(i) To estimate the plankton crop in a given water mass from a knowledge of the oxygen consumption.

(ii) To trace the origin of water masses and patterns of mixing.

(iii) To obtain information on the degassing of the earth.

It can be assumed that any water particle inside the sea has been at the surface and in equilibrium with air in the

past. When it sinks, it carries all the atmospheric gases dissolved in proportion to their solubilities at the temperature of contact. Many additional factors affect the gaseous contents of the water particle during its travel. Thus, a study of gas contents of deep water can in principle give information on the detailed processes which alter gas contents during travel of a water parcel.

Oxygen was the first gas to be investigated as a potential tracer of oceanic mixing and also as an index of biological activity. However, it proved difficult to estimate the oxygen consumption in a water mass, because of its generation by other sources, mainly photosynthesis and bacterial oxidation of organic matter. Many workers, since Buch (1) and Rakestraw and Emmel (2), have tackled the problem differently. These workers have assumed that the sea water concentration of inert gases should approximately correspond to solubility at the in situ water temperature. Therefore, if measurements are made of the concentration of a reference inert gas, whose solubility ratio to that of oxygen is already established, then the original atmospheric component of oxygen can be determined. Nitrogen and Argon have been used extensively in this way, although recent studies have included other rare gases. The results

obtained have suffered from one serious disadvantage, they have all depended heavily on the solubility data of the inert gases, which were few and lacked the required precision. However, with the recent availability of accurate solubility data (3, 4) the problem can be examined in a more quantitative way.

Helium is produced in the solid earth through the radioactive decay of uranium and thorium,

$$^{238}U \longrightarrow {}^{206}Pb + 8\ {}^{4}He$$

$$^{235}U \longrightarrow {}^{207}Pb + 7\ {}^{4}He$$

$$^{232}Th \longrightarrow {}^{208}Pb + 6\ {}^{4}He.$$

If the earth has the composition of chondritic meteorites (1.1×10^{-8} gg^{-1} of uranium, 4.4×10^{-8} gg^{-1} of thorium), then an upper limit for helium flux into the atmosphere is 3.0×10^{-6} cm^3 STP cm^{-2} yr^{-1}. Radiocarbon measurements of deep sea water give an "age" of approximately 1000 years (5), the time since deep water has equilibrated with atmospheric CO_2. Hence, a water column of 3900 meters (i.e. the average oceanic depth) should contain about 7.7×10^{-6} cm^3 STP of radiogenic helium per liter of sea water. This is about 19% of the average helium content of the bottom water i.e. 4×10^{-5} cm^3 STP/liter (6) and the predicted excess is easily measureable by modern mass spectrometric techniques.

On the basis of above considerations, Revelle and Suess (7) suggested that modern analytical methods might allow the detection of helium leaking through the ocean floor by measurements of "excess" helium in deep water compared to surface water. They also suggested that knowledge of temperature dependence of the solubilities, and careful measurements of the variations in the concentration ratio of several rare gases, would be of significant use in determining the mixing of water masses of different temperatures. For example, Xe is about 1.7 times as soluble in sea water at 0°C than at 20°C and the Xe/Ne solubility ratio is 13.6 and 9.15 respectively at those temperatures (see Fig. 1). That is, a slight change in temperature is more serious for Xe than for Ne concentrations. A mixture of equal proportions of saturated sea water at 0°C and 20°C would show $\Delta(Ne) = 1.16\%$ and $\Delta(Xe) = 4.86\%$, where Δ is the saturation anomaly defined by the following equation:

$$\Delta(\%) = [(C/C^*)-1] \times 100 \quad - - - - - - - - - - - - - - - \quad (1)$$

Here C is the gas concentration observed in a sea sample and C^* is the solubility equilibrium value at the potential temperature of the sea sample. Potential temperature is the temperature attained by a water sample that is raised adiabatically from a certain depth to the ocean surface.

Thus, comparison of Xe/Ne ratios at various temperatures would indicate the origin of the water masses that mixed together. Both these proposals marked the beginning of an era of serious and detailed investigations of rare gases dissolved in sea water.

B. PREVIOUS MEASUREMENTS

Measurements of helium and neon in the sea were first reported along with N_2 and Ar by König et al. (6) in 1964. Using an apparatus for microanalysis of rare gases developed by Paneth and Peters (8), they found an average of $(41.8 \pm 1.2) \times 10^{-6}$ ml/kg of helium and $(171.3 \pm 1.8) \times 10^{-6}$ ml/kg of neon in bottom water of north Pacific and south Indian Oceans. Their data show an upper limit of 10.6% for He excess and 4% for Ne excess relative to the solubility data of König (9), which are uncertain to $\pm 3\%$. However, the north Pacific deep water appeared to show helium enrichment of about $6 \pm 2\%$ relative to the south Indian Ocean deep water, which is explainable in terms of age of the water. Suess and Wänke (10) noted that the bottom water takes about 700 years to move from the south Indian Ocean to the north Pacific Ocean, and calculated

that the maximum difference could be as much as 18% for the helium of these oceans. However, the observed difference of 6 $\pm$ 2% was regarded by these authors as an upper limit because of the different sampling techniques used for the two oceans. The Pacific Ocean samples were first stored in pyrex cylinders which would be subject to He diffusion and the gases were sealed in soft glass after extraction, whereas the Indian Ocean water samples were transferred into stainless steel cylinders and extracted immediately before analysis.

Later, Mazor, Wasserburg and Craig (11) analysed four south Pacific water samples by isotope dilution mass spectrometry for all the rare gases. Except for helium, which was too high by a factor of six (because of helium diffusion through the pyrex glass sample tubes), the Ne, Kr, and Xe concentrations were generally consistent with König's solubility values (9) to about $\pm$10%.

Bieri, Koide and Goldberg (12) using an omegatron mass spectrometer without isotope dilution reported large variations from solubility equilibrium for all the noble gases in the Pacific Ocean. For helium and neon, they found values ranging between 75 and 125%, and 62 and 114% of saturation respectively. The same group again in 1966

(13) observed general supersaturation of helium, neon, argon and krypton at all depths in the Pacific; concentrations as high as 124, 112 and 115% of saturation were measured for He, Ne and Ar respectively. But this large supersaturation of argon was questioned by Craig et al. (14). They invoked the use of temperature-salinity (T-S) diagrams to explain small increases in saturation anomaly as the result of core properties of water types involved in subsurface mixing. For excess helium concentration, they gave 8.7% as a reliable upper limit for one sample at a depth of 1009m (32° 47'S, 72° 46'W). Their results on helium, neon and argon substantiate the work of König et al. and Mazor et al. That is, only minor (<10%) deviations from solubility were found.

In summary, the measurements of helium and neon in sea water have been accomplished by one of the three techniques; volumetric (6), mass spectrometer peak height measurements relative to standard air volumes (12, 13) and isotope dilution mass spectrometry (11, 14), the last method being the most reliable. The results also formed two groups; those within $\pm$10% of the solubility equilibrium (6, 11, 14, 15) and those with large supersaturations reported by Bieri et al. (12, 13). Moreover, there is a

common factor to all these measurements. They were all normalized either to the König's (9) solubility data, which are few in number and of relatively low precision, or to neon (in case of He) or argon data, which in turn were based upon approximate solubility values. The lack of good solubility data has contributed an unknown error to the results for saturation anomalies and helium flux calculations. The data on helium has also suffered from leakage problems. The problem of the existence of a real helium excess in the deep sea was far from settled when this work was initiated.

C. PRESENT APPROACH

In view of the factors outlined above, the work described in this thesis was initiated with a distinctly different approach. Instead of measuring the He content of sea water, it was decided to measure the $^3He/^4He$ ratio at various depths by means of a sensitive mass spectrometer. Assuming the same solubility for ^3He and ^4He, a higher $^4He/^3He$ ratio in deep waters relative to surface waters would indicate a ^4He flux through the ocean floor, and circumvent the necessity of using helium solubilities for this purpose. The first analyses of Pacific Ocean water

showed a ^3He excess relative to the atmospheric $^3He/^4He$ ratio in general (16, 17) with the largest excess (~20%) at mid-depths. Ratio differences are expressed in terms of $\delta(^3He)$ values, where

$$\delta^3He\ (\%) = \left[\frac{(^3He/^4He)_{sea}}{(^3He/^4He)_{air}} - 1\right] \times 100 \quad - - - - - - - - - - \quad (2)$$

These measurements showed that the surface waters (~500 m thick layer) are well mixed and the $\delta(^3He)$ observed can be accounted for by ^3He produced from artificial tritium decay added to the expected value, i.e. -1.4%, the ^3He solubility effect as measured by Weiss (18). The ^3He excess below the mixed layer could be explained only by supposing a mid-depth injection of ^3He. A weak correlation between $\delta(^3He)$ and $\Delta(He)$ was also noted for the Nova Expedition (31.0°S, 177.0°W) data (16). The $\Delta(He)$ measurements were less precise than the $\delta(^3He)$ values because of peak height comparisons but quite consistent with the $\Delta(He)$ data in the literature obtained by isotope dilution analyses (14, 15).

D. FACTORS AFFECTING RARE GAS CONCENTRATIONS

It is evident that variations in the rare gas contents from solubility equilibrium do exist in the sea.

Factors responsible for these variations have been discussed by Benson and Parker (19), Bieri et al. (13), Craig et al. (14), Craig and Weiss (20), König et al. (6), and Revelle and Suess (7). These factors are:

(i) Water temperature and salinity.

(ii) Air injection in the form of bubbles carried down to a considerable depth.

(iii) Changes in atmospheric pressure.

(iv) Radioactive decay and influx through the ocean floor.

The first three factors are interdependent and can lead to supersaturation or undersaturation of a gas, while the last factor will always lead to supersaturation.

Changes in the atmospheric pressure are at the most ±3% and have the same effect on all the gases (14). Air injection and temperature changes after gas equilibration have different effects on each gas. Because of its low solubility helium will be affected the most by air injection and least by temperature changes as compared to other rare gases. This can be better understood from Fig. 1 and Table I.

Table I, constructed from Weiss' (3, 4) and König's data (9), compares the solubilities of inert gases at 20°C and salinity = 35‰ with their concentration in air.

TABLE I

COMPARISON OF INERT GAS SOLUBILITIES (at S = 35 ‰, T = 20°C)

WITH THEIR CONCENTRATION IN AIR

Gas	Air* ml/l	Solubility in sea water ml/kg
He	52.4×10^{-4}	3.729×10^{-5}
N_2	780.8	9.28
Ne	181.8×10^{-4}	1.519×10^{-4}
Ar	9.34	0.2469
Kr	11.4×10^{-4}	51.1×10^{-6}
Xe	0.87×10^{-4}	6.88×10^{-6}

*Data taken from Gluekauf (21).

Solubility is defined as the volume of the gas (STP) absorbed from water saturated air at a total pressure of one atmosphere per unit volume (or mass) of the sea water at the temperature of the measurement. It is expressed as milliliter per liter (ml/l) or milliliter per kilogram (ml/kg) of sea water. The units ml/kg shall be used in this thesis, since they eliminate the ambiguities arising from temperature and pressure effects. Solubility is a function of temperature and salinity, the general relation for He, Ne, N_2 and Ar being (3, 4),

$$\ln C^* = A_1 + A_2\,(100/T) + A_3 \ln(T/100) + A_4(T/100) + S‰\,[B_1 + B_2(T/100) + B_3(T/100)^2] - - - - - - - (3)$$

where C* is the solubility in ml/kg (STP), the A's and B's are constants (different for each gas), T is the absolute temperature, and S‰ is the salinity in per mil. Salinity is related to chlorinity (3) (Cl ‰) by the following equation:

$$S‰ = 1.80655\ Cl\ ‰ \quad - (4)$$

Solubility can also be expressed in terms of β, the Bunsen solubility coefficient. It is defined as the volume of gas

(STP) absorbed per unit volume of liquid at the temperature of the measurement when the partial pressure of the gas is one atmosphere. β has exactly the same relationship to T and S as C^* has, except that the constants A and B are different. Roughly, β times the partial pressure (p) of a gas equals the concentration of the gas in sea water.

Fig. 1, based on Weiss data (3, 4), shows the temperature dependence of β for helium, neon and argon for S = 35 ‰. For comparison, the β values of Kr and Xe are also listed from König's data (9); they are not plotted because they are few in number and do not cover the temperature range uniformly. If a water parcel originating at 0°C in the Antarctic sinks down and reaches equilibrium on its northward travel at 20°C without coming into contact with the atmosphere the solubility coefficient β will decrease by about 41, 35, 13 and 5% respectively, for Xe, Ar, Ne and He; Δ will also go down proportionately. On the other hand, if a temperature drop occurs due to sudden weather changes or other phenomena, the solubility of the surface water for rare gases would increase causing supersaturation. As mentioned earlier, mixing of equal proportions of water masses at 0°C and 20°C would lead to increased Δ by about 1% for He and Ne compared to about 4.5% for Ar and Xe. Therefore the temperature variations have non-linear

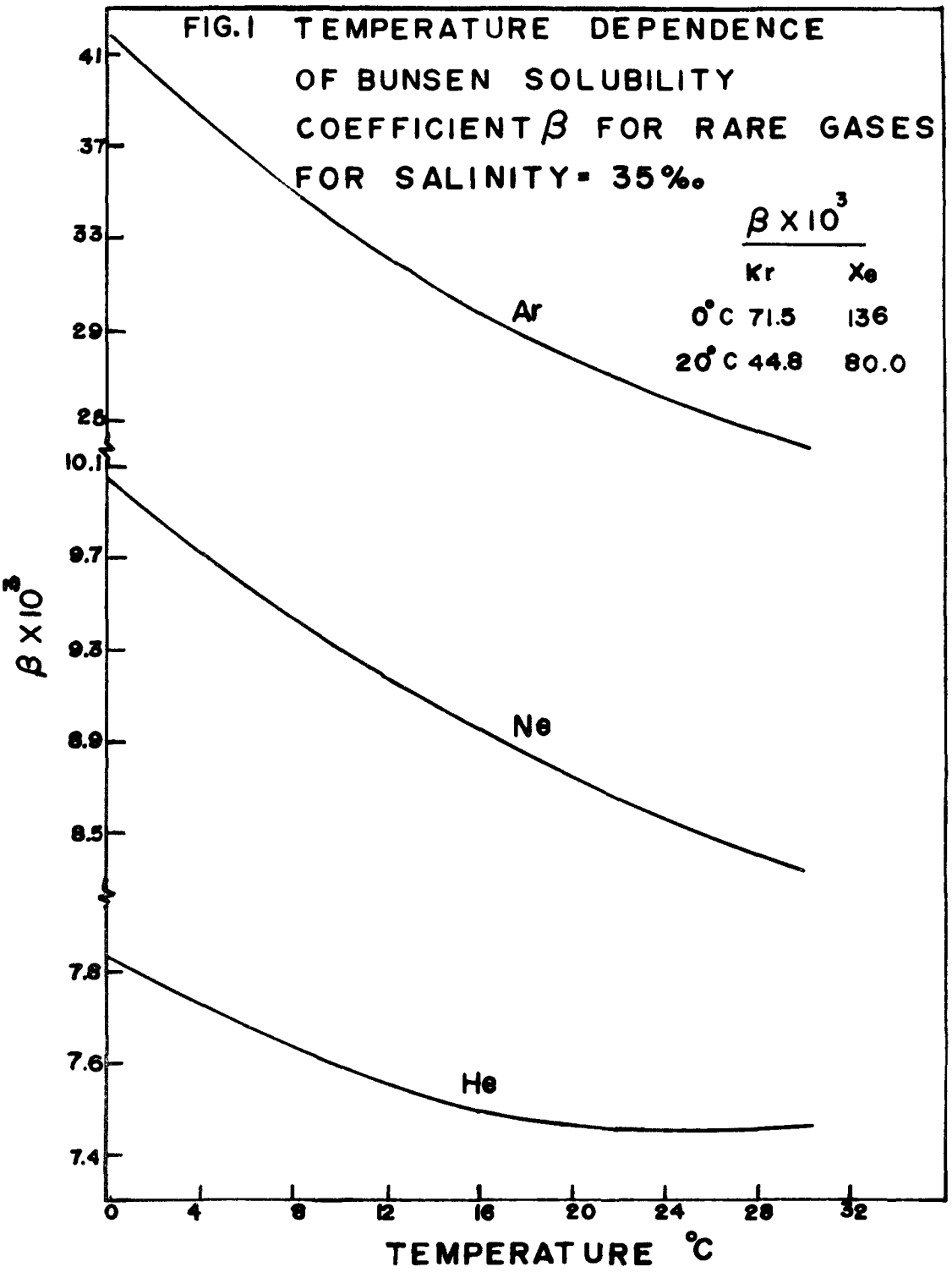
FIG. 1 TEMPERATURE DEPENDENCE OF BUNSEN SOLUBILITY COEFFICIENT β FOR RARE GASES FOR SALINITY = 35‰
β X 10³
Kr Xe
0°C 71.5 136
20°C 44.8 80.0
Ar
Ne
He
β X 10³
41
37
33
29
25
10.1
9.7
9.3
8.9
8.5
7.8
7.6
7.4
0 4 8 12 16 20 24 28 32
TEMPERATURE °C

effect on the solubility of gases with He being the least affected.

Air injection in the form of bubbles is mainly responsible for high Δ values as far as He and Ne are concerned. The ratio ($100\ p_o/C^*$) is an indicator of the extent to which Δ of a particular gas suffers if there is an air injection (20), where p_o is the concentration of the gas in air, and C^* is in ml/kg. Thus at 20°C and S = 35‰, an input of 1 ml/kg of air will lead to about 14, 12, and 3.8% increase in the saturation anomalies of He, Ne and Ar respectively. Since there is no known radiogenic or primordial Ne component in sea water, and temperature and pressure effects are approximately the same for He and Ne, the Δ(Ne) can be used to establish Δ' (He) as follows. From the preceding discussion, various contributions to Δ(He) are:

$$\Delta(\text{He}) = \Delta(\underset{\text{changes}}{\text{temp.}}) + \Delta(\underset{\text{changes}}{\text{pressure}}) + \Delta(\underset{\text{injection}}{\text{air}}) + \Delta'(\text{He}) \quad (5)$$

where

$\Delta'(\text{He}) \equiv \Delta(\text{radiogenic}) + \Delta(\text{primordial})$.

Assuming f[Δ(Ne)] equivalent to the first three effects given in equation (5), the Δ'(He) would be:

$$\Delta'(\text{He}) = \Delta(\text{He}) - f[\Delta(\text{Ne})]. \quad \text{- - - - - - - - - - - - - - - - -} (6)$$

The factor f is a function of the solubilities of the gases involved, i.e.

$$f = \left(\frac{p_o}{C^*}\right)_{He} \Big/ \left(\frac{p_o}{C^*}\right)_{Ne} \qquad \text{- - - - - - - - - - - - - - - - - - - (7)}$$

For the above quoted percentages for air injections, f would be (14/12) $\simeq$ 1.17.

Additional information obtained by ^3He measurements would be useful in:

(i) Fixing the well mixed surface layer for a station, thus any Δ(He) observed in this layer would be due to air injection only.

(ii) Estimating the radiogenic and primordial ^4He components if a correlation exists between $\delta(^3He)$ and Δ'(He).

It was with these possibilities in mind that the present work was carried out. Fortunately, since this work began, helium, neon and argon solubilities have been remeasured with more accuracy by Weiss (3, 4) and shall be used to compare the gas concentrations. In order to account for all the components of Δ(He) (see equation 5), measurements on at least three gases other than helium are required.

Therefore Ar-Kr-Xe fractions were also collected for all the sea water samples whose ^{3}He, ^{4}He and Ne measurements are reported in this thesis. When analysed, the Ar-Kr-Xe data coupled with ^{3}He, ^{4}He and Ne data should help in identifying precisely the magnitude of various components of the observed saturation anomalies of each gas.

CHAPTER II

EXPERIMENTAL

A. COLLECTION OF SEA WATER SAMPLES

Sea water samples for the work reported here were collected on the following expeditions.

(i) Expedition NOVA (Scripps Institution of Oceanography) in the south Pacific Ocean during September, 1967.

(ii) GEOSECS Expedition (1969 Test Station) in the north Pacific Ocean during September, 1969.

(iii) HUDSON 70 Expedition (Bedford Institute) in the south Atlantic Ocean during January, 1970.

(iv) SCAN Expedition (Scripps Institution of Oceanography) in the south Pacific Ocean during February, 1970.

Professor H. Craig of Scripps Institution of Oceanography collected the water samples during the NOVA, GEOSECS and SCAN Expeditions. Professor P. J. Wangersky of Dalhousie University collected the south Atlantic samples during the HUDSON 70 Cruise.

The water samples were collected in 300 ml and 500 ml stainless steel cylinders with steel stem tip (chrome-coated) valves, argon-arc welded to each end. The size

300 ml was chosen, so that the $^3He/^4He$ ratio in the sample relative to the atmospheric $^3He/^4He$ ratio could be determined with a precision of 1-2 % using the available mass spectrometer. The helium detection limit of this instrument is about 10^6 atoms. Therefore, for the required precision, the ^3He content in the sea sample should be $\gtrsim 10^8$ atoms; this is equivalent to the ^3He content of 300 ml of sea water (6) if the atmospheric ratio of $^3He/^4He$ of 1.4×10^{-6} (22) is assumed. However, water samples of even smaller size (50 ml) have also been analyzed successfully.

The initial batch of nine cylinders were carefully leak tested prior to the NOVA expedition by sealing them on to the inlet system of the mass spectrometer. While monitoring the ^4He peak, tank helium was directed at the valves and welds. Thus an upper limit of 10^{-10} cm^3 STP/min for the helium leakage rate was determined for each cylinder. For storage of the samples under wet conditions i.e. valve ends filled with water, the leak rate would be less than 10^{-13} cm^3 STP/year, which is entirely negligible compared to the sample volume of about 10^{-5} cm^3 STP of helium. The other cylinders were leak tested differently. Each cylinder was sealed on to a vacuum line and pumped to a pressure of 1×10^{-5} mm Hg. Ethanol was sprayed on the welds and valves but no change in the pressure was

observed. Therefore, these cylinders were assumed as leak-tight as the first batch, a fact that was substantiated by later helium measurements. After the leak test, every cylinder was well pumped out and filled with dry nitrogen at an excess pressure of about half an atmosphere. A torque of 50 to 70 inch-pounds was applied to each valve with a torque wrench.

Large thirty-liter Niskin as well as two-liter Nansen bottles were used for collecting all the samples, except surface water at the South Pacific NOVA station, which was collected underway through the sea chest inlet line in the bottom of the ship. The sample cylinders were filled from the Nansen or Niskin bottles immediately as each bottle arrived on deck, using a simple gravity flow system with Tygon tubing and Swagelock fittings. The sample cylinders were held upright and filled through the bottom valve, after the top valve had been opened into a plastic line, the other end of which was immersed in a large beaker of sea water through which the nitrogen bubbled out. The inlet line and outer section of the bottom valve were flushed briefly and connected and the sample cylinder was flushed with 500 to 900 ml of sample water, depending on the size of the cylinder, before closing off the valves and tightening with a torque wrench. During

the filling the upper valve of the Nansen or Niskin bottle was always open to the atmosphere, to prevent degassing inside the bottle. The outer tabulations of the valves on the sample cylinders were filled with sea water and closed off with threaded metal caps for storage.

For total helium and neon studies by isotope dilution, another type of sampler was used. It is the Piggyback sampler (23), which essentially consists of a length of soft annealed copper refrigeration tubing (3/8 in. od. x 0.032 in. wall) containing the water sample (~17 ml) and clamped at both ends by pinch clamps. This sampler attaches directly to a standard Nansen bottle and the valves at each end are activated by the tripping of the Nansen bottle. Thus the Piggyback sampler collects water at the same time and place at which the Nansen bottle collects water for other studies. When the sampler arrives on board, it is removed from the Nansen bottle without opening the valves, two pinch clamps are mounted near each end and tightened until the ends of the bars forming the clamps just touch. Then the valves are removed from the sampler, both ends are filled with sea water or tap water and stoppered for storage. Mass spectrometer leak tests were carried out for these seals, and indicated that the

seals are so good that under wet conditions the leakage rate is less than 2.6×10^{-13} STP/year, about the same as the upper limit determined for the leakage rate of cylinders. Despite the tightness of the seals, samples are easily opened for analysis. When the seal is to be opened, the clamp is removed and the tube is partially re-rounded using the hole in the clamp intended for that purpose.

B. EXTRACTION OF RARE GASES FROM SEA WATER

Rare gases from water samples were extracted in a vacuum line similar to that described by Craig, et al. (14) with some modifications. The method consists of outgassing the sea water in a vacuum system, where the He-Ne fraction can be separated from other gases, collected into a sample tube by means of a Toepler pump and the Ar fraction collected in a charcoal break seal tube after purification by hot (700°C) titanium.

The extraction line is schematically shown in Fig. 2. To minimize atmospheric helium diffusion during an extraction, the line and the He-Ne sample tubes were

FIG·2 EXTRACTION LINE FOR RARE GASES

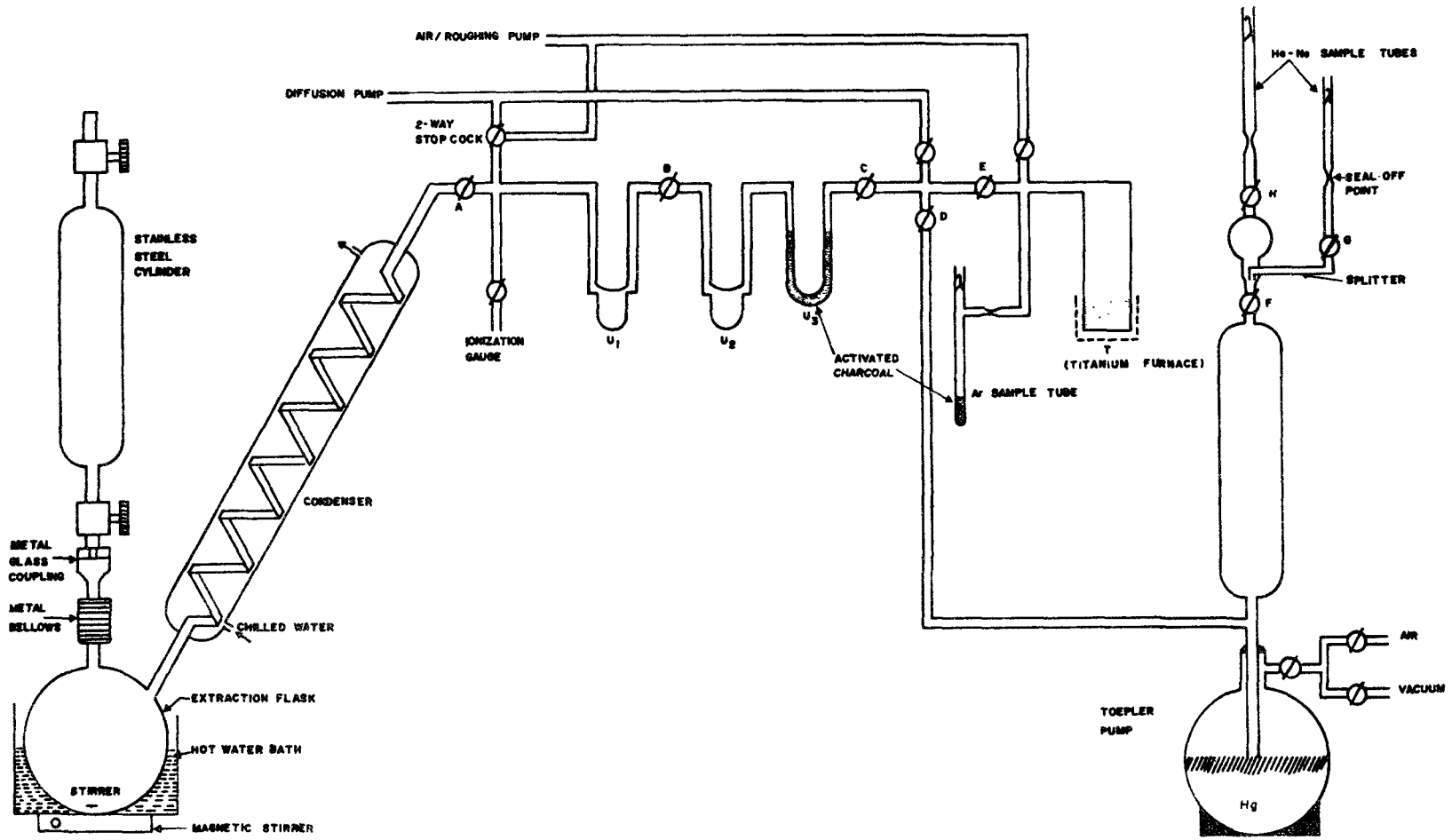

constructed from Corning 1723, a glass of exceptionally low helium permeability (24). The extraction flask, chilled water condenser and Toepler pump were made of soft glass. The argon sample tube, titanium furnace glass section and stopcocks were of Pyrex. High vacuum stopcocks of the type with a glass bulb at the bottom were used during the course of this project. The line could be pumped down to a pressure of 1×10^{-5} torr, monitored by an ionization gauge. Extraction flasks of two different sizes (1000 ml and 140 ml) were used, depending upon the size of the water sample. A Teflon covered stirrer, operated from outside by a magnetic stirrer, was placed in the flask before glass blowing. Connection of the water sampler to the extraction flask was made by a Teflon taped threaded metal to glass coupling for cylinders and a Viton O-ring seal for Piggyback samplers.

In order to carry out ^{3}He-^{4}He and He-Ne measurements on the same water sample, an accurately calibrated sample "splitter" was incorporated at the final stage of the He-Ne collection, to split all the samples except the Piggybacks into two fractions with relative volume of 14.83:1. The big fraction was used for ^{3}He-^{4}He measurements, while the small fraction was used for determination of total He

and Ne. Piggyback samples (~17 ml) were too small for precise ^3He measurements, and were only used for He-Ne determinations.

The various steps of the extraction procedure were as follows.

(i) The water sampler was accurately weighed and joined to the extraction flask to which about 30 mg of solid P_2O_5 had been added.

(ii) The extraction line was pumped down to a pressure of 5×10^{-5} torr, titanium furnace T switched on, and the argon recovery tube and U_3 flamed. The amount of charcoal in U_3 was sufficient to completely withhold Ar and other gases but allowed free passage of Ne and He at liquid N_2 temperature (-196°C). The stoppers of the stopcocks were turned around a few times to release any gases dissolved in the silicone grease.

(iii) When the splitter was in use, a few drops of Hg were left above G and H, the stopcocks closed, and Hg brought down to its usual level in the Toepler pump before an extraction was started.

(iv) Chilled water (at ~2°C) circulation was started through the condenser.

(v) E was closed, the extraction line was isolated from the diffusion pump and ionization gauge, B closed, and the dry ice bath raised on U_1.

(vi) The water sample was let in slowly into the extraction flask, the magnetic stirrer started, and water at 60°C added to the hot water bath. The bath was kept at this temperature during extraction.

(vii) Liquid N_2 was placed on U_2 and U_3. After five minutes B was opened and collection of He-Ne started; the gas sample was pushed into the splitter by Toepler pump, F closed and Hg lowered for the next stroke. The Toepler pump was operated about 20 times.

(viii) Half way through the extraction, A and B were closed, U_1 defrosted to ensure free passage of gases, the coolant put back on U_1, A and B opened, and extraction continued. Before the last stroke of the Toepler pump, B was closed and U_2 defrosted.

(ix) The final stroke was collected by raising the Hg very slowly across F until it cut the splitter edge evenly and reached the middle of the splitter. G and H were then opened, Hg drops above them let down, and Hg raised up to the seal-off point of the sampler tubes.

(x) F, G, and H were closed and He-Ne sample tubes sealed off as close as possible to the Hg surface.

(xi) Without lowering Hg, C and D were closed, U_3 defrosted and flamed, C, D, and E opened and the Ar sample tube flamed.

(xii) After five minutes the titanium furnace was switched off. When the furnace was cool, the purified Ar was condensed over charcoal at liquid N_2 temperature and the tube sealed off.

The whole process of extraction was completed in about 45 minutes. Blank extractions were done in which all the above steps were carried out except that there was no water let into the system. Tests were also made for extraction efficiency by repeating the process with a degassed water sample. Analysis showed that extraction efficiency of all samples was better than 99.9% for He and 99.5 $\pm$ .2% for Ne; the line blanks were <1% for Piggybacks and <0.1% for cylinders. All the sample break-seals were stored at room temperature, and for some of them, Hg was placed on top of the break-seal to minimize He diffusion from the atmosphere.

After each extraction, the water from the extraction flask was siphoned out and the flask was flushed with distilled water to remove the salt left on its walls. The last traces of water in the flask and U_1 were pumped out by a rotary pump capable of handling water vapour. The empty sample cylinders were rinsed with distilled water, dried overnight in an oven, cooled and then weighed to obtain the weight of the sea water. Piggyback sample tubes were dried by a brief pump-out and weighed soon after extraction.

C. PREPARATION OF CALIBRATED SPIKES

The isotope dilution method is an important technique for the determination of absolute contents of gases or solids. By adding a known number of atoms of a separated isotope of an element under study, and then measuring by means of a mass spectrometer the isotopic ratios, it is possible to calculate the absolute number of atoms which were present in the original sample. Total He and Ne contents of sea water were determined by mixing accurately calibrated spikes of ^{3}He and ^{22}Ne with the He-Ne fractions. It was decided to intersperse measurements of the spiked samples with

measurements of standard mixtures of ^{3}He, ^{4}He, ^{20}Ne and ^{22}Ne of known $^{4}He/^{3}He$ and $^{22}Ne/^{20}Ne$ ratios. This procedure simultaneously determined the mass discrimination factor of the mass spectrometer for $^{4}He/^{3}He$ and $^{22}Ne/^{20}Ne$, as well as the reproducibility of the measurements.

The size of the sea samples under consideration was approximately 20 ml, containing approximately 8.0×10^{-7} cc STP of He and 36×10^{-7} cc STP of Ne (6). Therefore, He and Ne spikes of about the same size were prepared from each pure gaseous isotope in order to produce spike mixtures of (^{3}He + ^{22}Ne) and standard mixtures of (^{3}He + ^{4}He + ^{20}Ne + ^{22}Ne), with $^{4}He/^{3}He$ and $^{22}Ne/^{20}Ne$ ratios roughly equal to one. The ^{3}He (99.99% pure), ^{20}Ne (99.96% pure) and ^{22}Ne (99.8% pure) used were supplied by Monsanto Research Corporation, while pure ^{4}He was obtained from evaporating liquid helium. Both the spike mixtures were prepared independent of each other, stored at room temperature in Corning 1723 glass sample tubes, and mixed with sea samples immediately before mass spectrometric analyses.

All the spike preparations were carried out on the gas spike line shown in Fig. 3A. It was a high vacuum Pyrex glass line, consisting of two volumes V_1 (5.0104 $\pm$ .0022 ml) and V_2 (5227.5 $\pm$ 1 ml) with stopcocks lubricated with

FIG·3 GAS SPIKE LINE

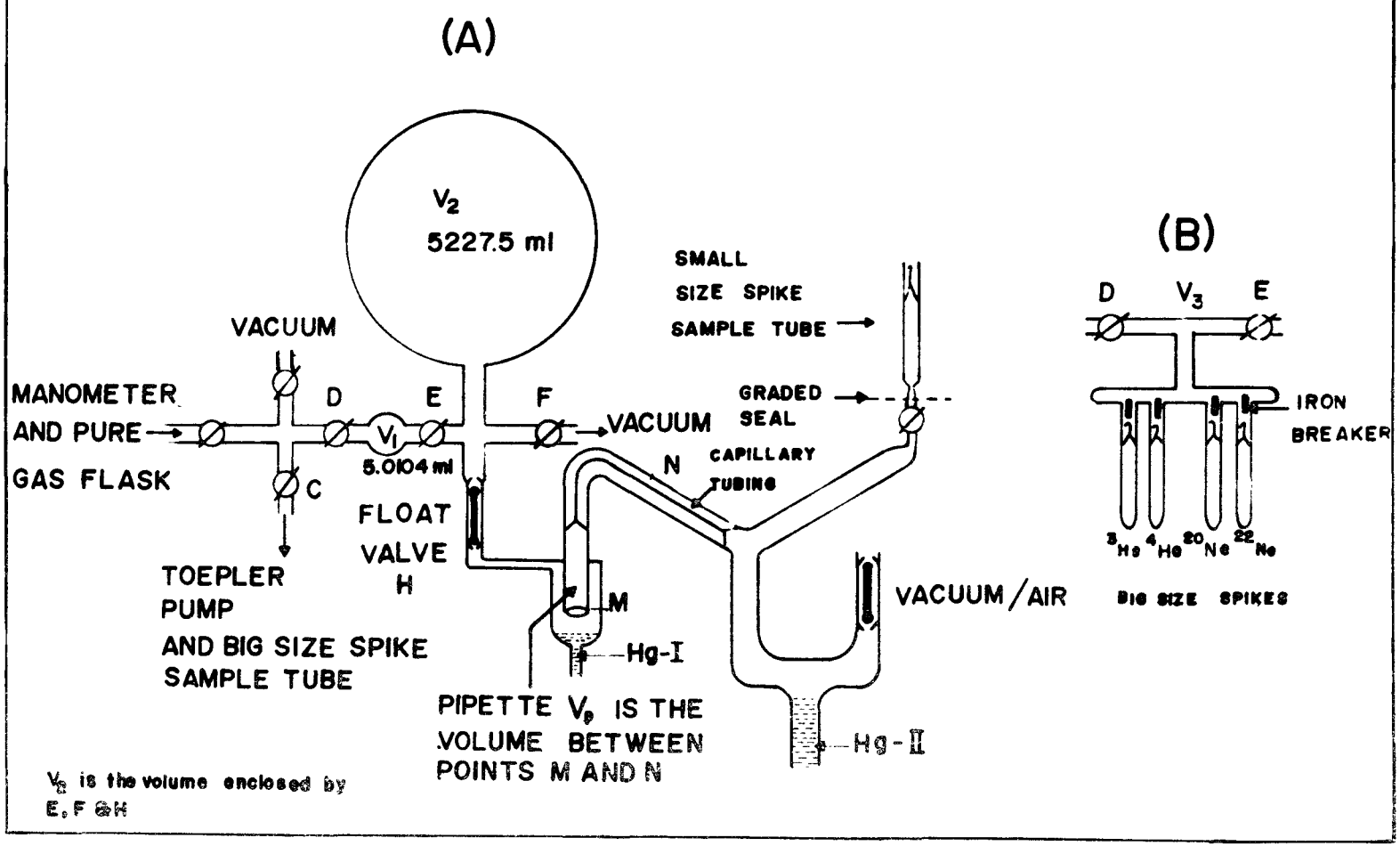

silicone grease and a mercury-operated pipette V_p (1.4110 $\pm$ .0018 ml). The line could be pumped down to a pressure of 2×10^{-6} torr. Depending upon the required size of a spike, a certain volume of tracer gas at a desired pressure (P_1 cm) and temperature (T_1°K) was first isolated in V_1, and later expanded into V_2 with F and H closed. After waiting about 30 minutes for the gas to reach equilibrium in ($V_1 + V_2$), E was closed.

Because the spikes involved were of very small sizes, they were prepared in two stages. First, big size spikes of each gas were prepared by taking aliquots in V_1 from V_2 and sealing them in sample tubes via stop cocks D and C and a Toepler pump. Later, the volume V_1 was replaced by V_3 (see Fig. 3B) and big spikes of two to four isotopes were sealed on depending upon the kind of mixture to be produced; V_3 would vary accordingly. The required small size mixture was collected by closing F, expanding gases into V_2, closing E and pipetting an aliquot of the mixture via V_p into the sample tube by operating the Hg-levels. One pipette of gas was taken by raising Hg-II to the file mark N, lowering Hg-I to below M and allowing sample into the pipette. Waiting ~30 sec for gas equilibration, Hg-I was gently raised across M until H was closed and the spike trapped

between Hg surface and N. Subsequently Hg-II was lowered and spike collected in the sample tube by Toepler pump operation.

The size of the first small spike prepared from the first big spike of a gas can be computed from the following equations:

$$S_1 = \left(\frac{V_1 P_1 T}{P T_1}\right)\left(\frac{V_1}{V_1+V_2}\right)$$

$$s_1 = S_1\left(\frac{V_2}{V_2+V_3}\right)\left(\frac{V_p}{V_2+V'+V_p}\right)$$

where S_1 and s_1 are the sizes of first big and small spikes respectively, P = 76 cms, T = 273°K, and V' = 10.7 ml, the extra volume for pipetting between V_2 and the cutting edge M. The prepared sizes of (^3He + ^{22}Ne) mixtures were accurate to $\pm$0.3% and within 10% of the He-Ne sea water contents. The $^4He/^3He$ and $^{22}Ne/^{20}Ne$ ratios in the standard mixtures were 1.4470 $\pm$ .0030 and 1.0208 $\pm$ .0020 respectively. Isotopic and chemical purity of the spikes will be discussed later.

D. MASS SPECTROMETRY

1. The Mass Spectrometer

The helium and neon isotope analyses were performed on a 90°, 10-inch, first-order direction focussing mass spectrometer shown schematically in Fig. 4. Source and collector slit widths of 0.1 mm and 0.3 mm provided a resolution of 620, sufficient for clean separation of ^{3}He from $HD\text{-}H_3$, $^{20}Ne^{+}$ from $^{40}Ar^{++}$ and $^{22}Ne^{+}$ from $^{12}C^{16}O_2^{++}$. In the ion source helium and neon are ionized by electron bombardment and accelerated to 2 kV. Before striking the first dynode of a 9-stage Cu-Be Allen-type electron multiplier, the ions are further accelerated by a potential difference of 3 kV. The current output of the electron multiplier is amplified by a vibrating reed electrometer (VRE) and fed to a chart recorder. However, for precise measurements, the signals from the VRE were also fed to a voltage-frequency converter, followed by an electronic counter and a printer which allowed integrated ion currents to be presented in digital form. The information was also displayed on a strip chart in analogue form.

Because of low ^{3}He ion currents (100 ions/sec) to be expected from a sample size of 10^{-11} cc STP, and possible

FIG. 4 MASS SPECTROMETER AND SAMPLE INLET SYSTEMS

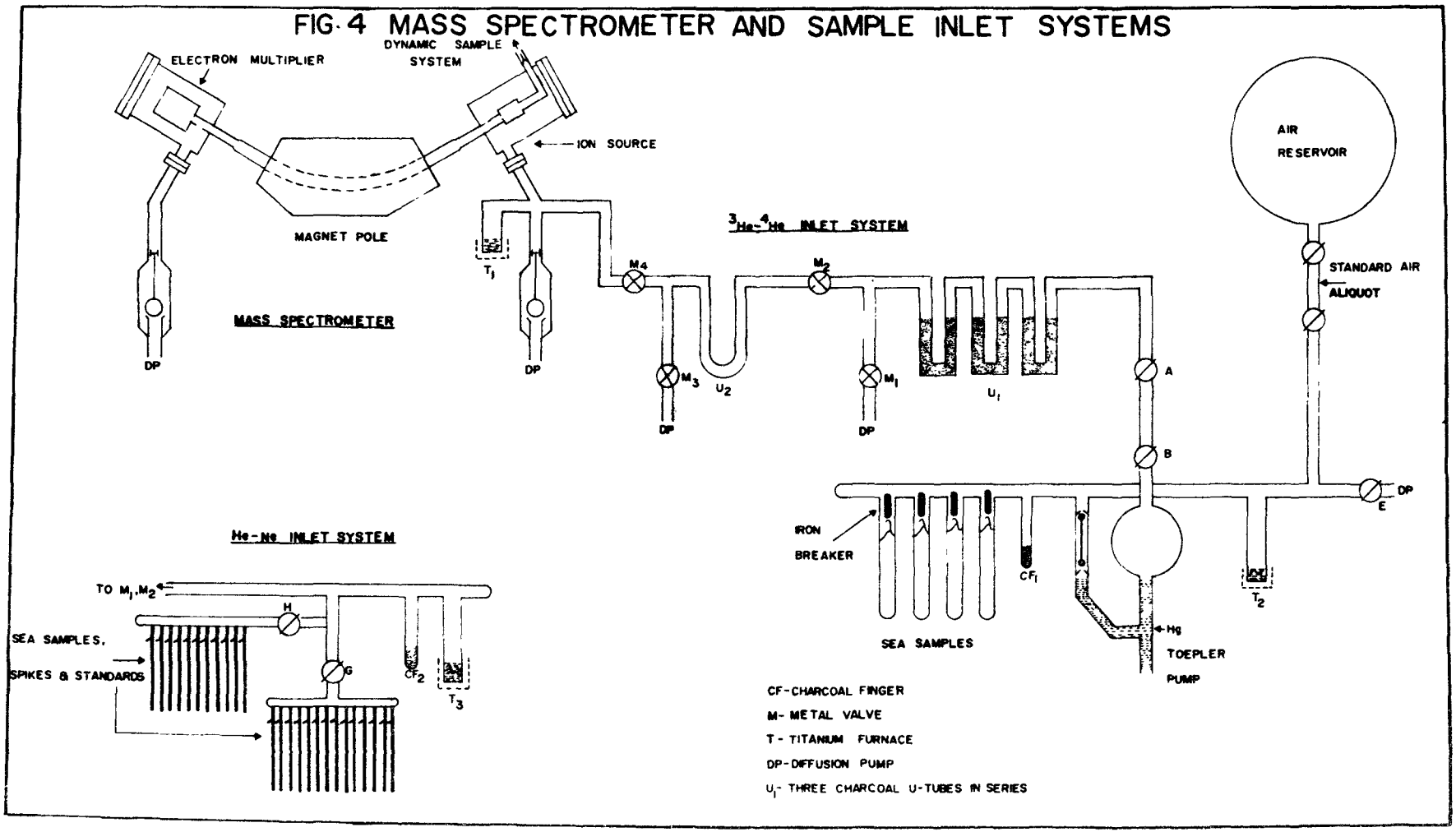

interference from the HD-H_3 peak, a few improvements were necessary to achieve maximum helium sensitivity. The static volume of the instrument was reduced by about 25% by filling the empty space in the source and collector regions with solid stainless steel cylinders having axial holes for pumping. The gain of the electron multiplier was increased from 10^4 to 3×10^5 by adding two more dynodes to the already existing nine, and reactivating by heating in hydrogen at 600°C. After many months of continuous operation, the gain stabilized to a value of about 10^5. Titanium furnace T_1 (see Fig. 4), containing a few grams of titanium was sealed to the static volume of the mass spectrometer. When out-gassed at 700°C and then allowed to cool to room temperature before a series of analyses, it acted as an efficient "getter" for H_2 released inside the instrument. HD and H_3 were kept at tolerable levels in this way.

2. Sample Introduction and Measurement Techniques

Two different high vacuum Pyrex glass sample inlet systems shown in Fig. 4 were used for ^3He-^4He and He-Ne analysis. The various steps of sample introduction for each type of analysis are described below.

(a) ^3He-^4He Analysis

The sea water samples for ^3He-^4He measurements were interspersed with standard air aliquots of roughly equivalent size (i.e. 1.2×10^{-5} cc STP ^4He) pipetted from an air reservoir. The air standards or gases (He-Ne fraction) extracted from sea water samples were purified in the ^3He-^4He inlet system, collected between a reproducible volume AB, and exposed to a series of charcoal traps U_2 at -196°C to hold back Ne. The helium was allowed to flow into the static instrument via M_4 for 30 seconds. This timing was closely reproduced for every air and sea sample. It was found that with this procedure 96 $\pm$ 1% of the total helium was admitted, and about 25% of neon, resulting in an increase of about 30% for helium ion currents compared to ion currents found when all the neon was admitted. The detailed procedure was as follows:

(i) The sample inlet system was pumped down to a pressure of $\sim 10^{-7}$ torr, CF_1, U_1 and T_2 degassed, and E and M_1 closed. Mercury was raised to the level shown in the diagram.

(ii) An air aliquot or sea sample (He-Ne fraction) was admitted, purified over CF_1 at -196°C and hot T_2, and pushed into the volume AB by Toepler pump.

(iii) M_3 was closed, and the sample allowed to flow for 30 seconds through U_1 and U_2 held at -196°C.

This whole process required about 10 minutes; the sample line blank for this much time was found to be <0.1% of the sample size.

The isotopic ratio measurements were carried out by switching the accelerating voltage back and forth from the middle of ^3He peak (~2.7 kV) to the middle of ^4He peak (~2 kV); their peak top widths were 2.0 and 1.7 volts respectively. Although small drifts in the magnetic field, equivalent to about 0.1 volt, were observed during the time of analysis (about one hour), flat-topped peaks were always obtained and such drifts had negligible effect on the ratio measurements. Fig. 5 shows a typical spectrogram obtained for ^3He-^4He analysis. ^3He and ^4He peak tops and their backgrounds were scanned for 100, 10 and 10 seconds respectively. The time at which each He^4 peak was measured was noted, with zero time equivalent to the time of closing the mass spectrometer valves.

(b) <u>He-Ne Analysis</u>

The samples for He-Ne content measurements were spiked with (^3He + ^{22}Ne) mixtures in the He-Ne inlet system

FIG·5 TYPICAL SPECTROGRAM FOR HE3–HE4 ANALYSIS

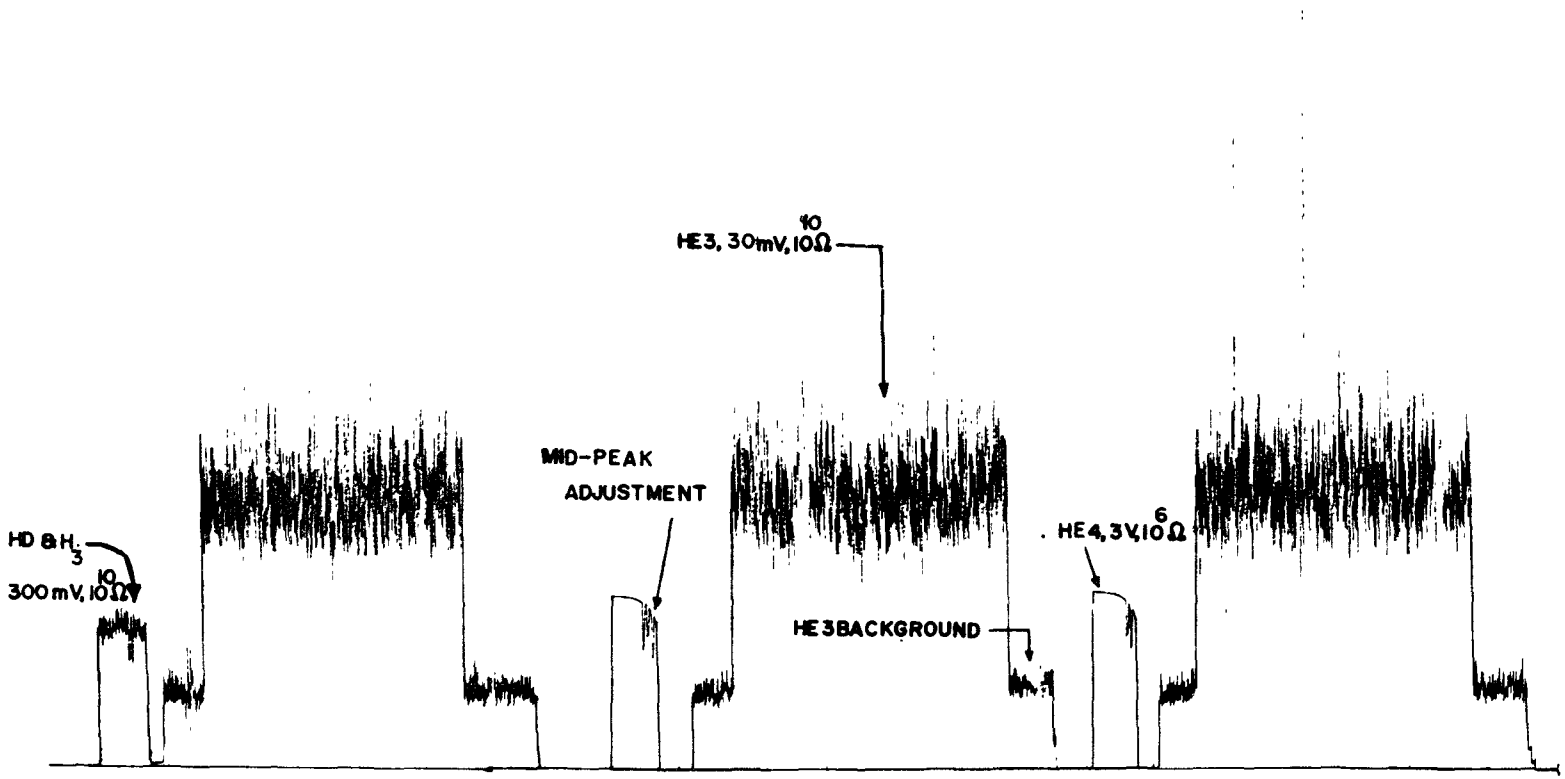

(see Fig. 4) prior to their analysis. Every sample was purified over CF_2 and T_3 by the usual methods, then the entire sample was admitted into the static mass spectrometer via M_2 and M_4. The details of the method were similar to those described for ^3He-^4He analysis except that the pure gas mixtures (^3He + ^4He + ^{20}Ne + ^{22}Ne) of known isotopic ratio were used as isotopic standards instead of atmospheric helium. The He-Ne inlet system helium blank amounted to ~0.3% of the usual sample size (~8 x 10^{-7} cm^3 STP He).

It was found that for samples of this size the ^4He background in the static volume of the instrument rose quite rapidly, as much as 5% of the sample size in 10 minutes, due to permeation of the atmospheric helium through glass parts of the mass spectrometer. Therefore the ^3He and ^4He peak tops (10 seconds wide) were scanned for 10 minutes only. After changing the magnetic field for neon isotopes, the scanning of ^{20}Ne and ^{22}Ne (also 10 seconds wide) was commenced and continued for another 20 minutes. Fig. 6 shows a complete chart record and peak shapes for a typical He-Ne analysis; it also indicates the ^4He permeation mentioned above, constancy of Ne peak heights and the decrease of ^3He peak height as a function of time.

FIG·6 TYPICAL SPECTROGRAM & PEAK SHAPES FOR HE–NE ANALYSIS

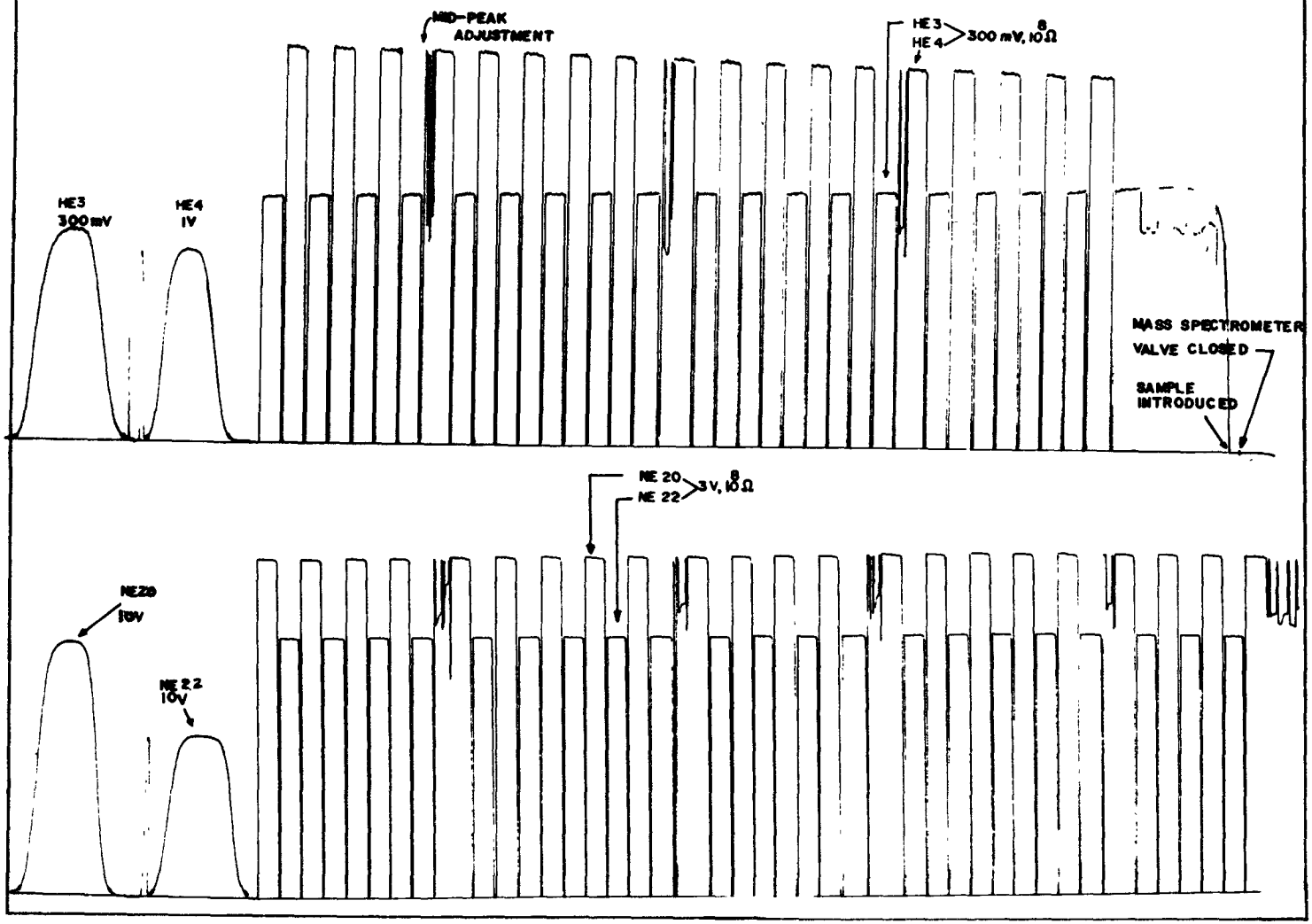

The last effect was due to preferential leakage of ^{3}He through the mass spectrometer valves. The time lag between closing the mass spectrometer valves and sample introduction does not introduce appreciable error into the extrapolated values for $^{3}He/^{4}He$.

The $^{40}Ar^{++}$ and $^{12}C^{16}O_2^{++}$ background contribution to $^{20}Ne^{+}$ and $^{22}Ne^{+}$ peaks respectively were found to be negligible under the experimental conditions. No trend with time in the mass spectrometer was observed for $^{20}Ne/^{22}Ne$ in samples analysed in this fashion. Hence quoted results for $^{20}Ne/^{22}Ne$ are mean values.

E. SOURCES OF ERROR

1. Chemical and Isotopic Purity of Spikes

The measured He and Ne contents were corrected for impurities, either chemical or isotopic, in the (^{3}He + ^{22}Ne) spikes used for isotope dilution. As far as chemical purity was concerned, only the Ne contents needed correction; they were increased by (0.3 $\pm$ 0.1)% for the presence of H_2 in the ^{22}Ne spikes. The isotopic impurity of the (^{3}He + ^{22}Ne) spike mixtures was determined from analysis for the presence

of ^{4}He and ^{20}Ne. Thus the He and Ne contents were reduced by (0.4 $\pm$ 0.2) and ~0.17% respectively for all the spiked samples excluding 50 ml samples, where the error was ~5 times higher.

2. Memory Effect and ^{4}He Background

Generally, when large size samples are analyzed on a mass spectrometer some of the sample atoms are left embedded in the walls of the instrument. These residue atoms will affect the results obtained for succeeding samples if they are of different isotopic composition. The memory effect is enhanced when the mass spectrometer is used in the static mode. During the present investigations a large ^{3}He memory effect was found because of prior analyses of samples heavily spiked with ^{3}He, whereas the instrument memory for ^{4}He and neon isotopes was negligible. Before a series of analysis it was necessary to reduce ^{3}He memory to tolerable levels. This was achieved by flushing the instrument repeatedly with dry nitrogen or argon at pressures of 10^{-6} to 10^{-5} torr over several hours with the ion source turned on, and baking afterwards at 300°C. For severe memory, the analyzer tube was scanned very slowly on either side of the collector slit with a N_2 beam to knock out imbedded ^{3}He atoms with the accelerating and electron multiplier voltages

switched on. However, the N_2 beam was not allowed to hit the first dynode for more than a few minutes so as to avoid a drop in the electron multiplier gain.

After each attempt to remove memory in the instrument, careful checks were carried out to determine whether $^3He/^4He$ analyses could be commenced. When the instrument valves were closed, with no sample admitted, the background ^3He and ^4He peaks would rise, due mainly to leakage of atmospheric He through glass sections. An anomalous component of ^3He could easily be detected by measuring $^3He/^4He$. After many days of "scrubbing" the instrument, when the anomalous component of ^3He appeared small, an air sample of similar size to the sea water (helium) samples was admitted and its behaviour ($^3He/^4He$ versus time) checked. The process was continued until the behaviour of air samples was identical to that of samples analysed when no memory component was present.

The slight ^3He leakage through one of the mass spectrometer valves and rise in the ^4He background observed during He-Ne studies were corrected by extrapolating all the measured isotope ratios back to zero time, when the mass spectrometer valves were closed and these effects were non-existent.

3. Mass Discrimination

The ion currents recorded for isotopic abundance measurements are discriminated as a function of the isotope mass at the ion source and the electron multiplier. The discrimination is more significant if the accelerating voltage is used to scan the isotopes, because the lighter isotope is favored by the ion source as well as the electron multiplier. Thus the observed $^4He/^3He$ and $^{22}Ne/^{20}Ne$ ratios are lower than their true ratios. The effect on helium ratios is quite pronounced since ^3He and ^4He were 700 volts apart (see section D, 2 (a)). The total He-Ne contents have been corrected for mass discrimination; the correction was not applicable to $\delta(^3He)$ (see equation (1)) measurements as the discrimination factor would affect the $(^3He/^4He)_{sea}$ and $(^3He/^4He)_{air}$ equally.

4. Measurement Errors

The errors in peak height measurements are mostly the consequence of statistical fluctuations in the ion currents. Therefore, to achieve better precision ten or more double scans were taken for each sample. For $^3He/^4He$ measured for atmospheric or sea water helium undiluted with ^3He, or for sea water helium "spiked" with ^3He and standard

$^{3}He/^{4}He$ mixtures, the errors quoted for isotopic ratios are one standard deviation of zero-time intercepts from a least squares fit of a plot of isotopic ratios versus time. The errors quoted for the neon isotopic ratios, both for sea water neon "spiked" with ^{22}Ne, and for standard $^{22}Ne/^{20}Ne$ mixtures are one standard deviation of the mean, i.e.

$$\sigma = \left(\frac{\Sigma (x_i - \bar{x})^2}{N(N-1)} \right)^{1/2}$$

where $\bar{x}$ = mean of N measurements,

N = number of measurements.

The He and Ne results reported in Chapter III have been corrected for various errors described in this section and elsewhere.

CHAPTER III

RESULTS

A. TOTAL HELIUM AND NEON MEASUREMENTS

The ^4He data were obtained from a plot of the $^4He/^3He$ ratios versus ^4He peak timings and finding the zero-time intercepts $(^4He/^3He)_{t=o}$ from least squares fit analysis, choosing a 95% confidence limit. An individual datum point of helium (or neon) ratios is equivalent to the ratio of ^4He peak height to the average of its two neighbouring ^3He peak heights, i.e., for a sequence of $^3He_1$ $^4He_1$ $^3He_2$ $^4He_2$ $^3He_3$ ..., the successive ratios are $[^4He_1/\frac{1}{2}(^3He_1 + {}^3He_2)]$ and so on. The total helium contents of the sea samples were computed by correcting their $(^4He/^3He)_{t=o}$ ratio for mass discrimination (analyses of sea water-spike mixtures were interspersed with analyses of accurately known $^3He/^4He$ standards) and multiplying by the size of the ^3He spike. In the case of neon contents, the $^{22}Ne/^{20}Ne$ ratios did not exhibit any variation with time, therefore no zero-time extrapolation was necessary. Instead, a grand average of the individual ratios was taken, mass

discrimination correction applied and the total neon contents then calculated, assuming Eberhardt et al's data (25) for atmospheric neon isotopic composition.

It is assumed that all the neon dissolved in sea water is of atmospheric origin, having the same isotopic abundance ratio. Thus a comparison of the measured $(^{22}Ne/^{20}Ne)_{sea}$ ratio with the $(^{22}Ne/^{20}Ne)_{air}$ would yield the neon content as described in the following. As sum of the ^{20}Ne, ^{21}Ne and ^{22}Ne abundances normalized to ^{20}Ne, abundance is:

$$(\Sigma Ne)_{air} = 1.0000 + 0.0030 + 0.1020 = 1.1050 \equiv (\Sigma Ne)_{sea},$$

therefore any $(^{22}Ne/^{20}Ne)_{sea} > 0.1020$ would be due to the ^{22}Ne spike used with the sea sample for isotope dilution. Hence,

$$\frac{(\Sigma Ne)_{sea}}{(^{22}Ne \text{ spike size})} = \frac{(\Sigma Ne)_{air}}{\left[\text{corrected}\left(\frac{^{22}Ne}{^{20}Ne}\right)_{sea} - \left(\frac{^{22}Ne}{^{20}Ne}\right)_{air}\right]},$$

or the total neon content of the sea water is:

$$(\Sigma Ne)_{sea} = \frac{(1.1050)(^{22}Ne \text{ spike size})}{\left[\text{corrected}\left(\frac{^{22}Ne}{^{20}Ne}\right)_{sea} - 0.1020\right]} \quad - - - - - - - - \quad (8)$$

The solubility C^* for each sample calculated according to equation (3) from T and S data was used to compare the He and Ne contents and compute respective Δ from equation (1). The results for He and Ne contents, Δ(He), Δ(Ne), Δ'(He), (see equation (6)), and other pertinent data are listed in Tables II - V for all the sampling stations. Their geographical locations are shown in Fig. 7 and Fig. 8; the latter shows the stations 35, 38, 41 and 56 over the East Pacific Rise (SCAN Expedition). The T-S diagrams for GEOSECS, NOVA and HUDSON 70 stations are drawn in Fig. 9; the GEOSECS profile is very similar to the one already reported (26) for this location. The points of inflexion in these diagrams indicate cores of different water masses entering the sampling region.

B. HELIUM-3 MEASUREMENTS

The ^3He data were obtained in a similar fashion to the ^4He data; the quoted $(^3He/^4He)_{t=o}$ ratios being the zero time intercepts found from plots of $^3He/^4He$ versus time. Fig. 10 shows one of these plots for a sea sample (2573 m, SCAN Expedition) and an immediately following air sample, clearly indicating that the ^3He excess is real. The


FIG·7 WATER SAMPLING STATIONS
60°
40°
20°
0°
20°
40°
60°
NORTH AMERICA
GEOSECS
SCAN
SOUTH AMERICA
NOVA
HUDSON 70
PACIFIC OCEAN
ATLANTIC OCEAN
ANTARCTICA
180°
160°
140°
120°
100°
80°
60°
40°
20°

FIG·8 SCAN EXPEDITION

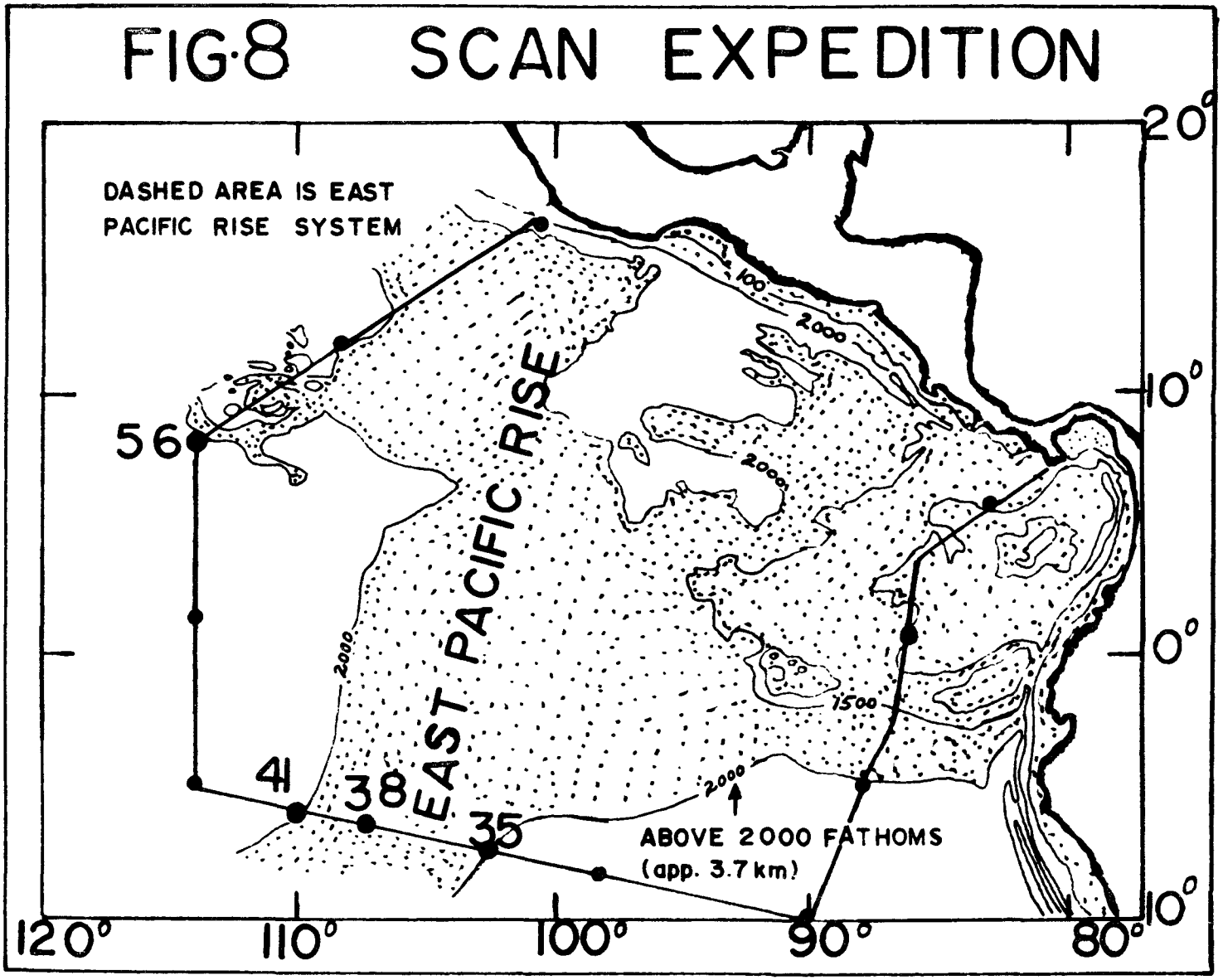

TABLE II. He-Ne DATA FROM NOVA EXPEDITION, STATION ARGO VI-2; 31.0°S, 177.0°W, 24 September, 1967.

Sampler	Depth (m)	Salinity ‰	Potential Temp. (°C)	He Content cc STP/kg x 10^5	Δ(He) %	Ne Content cc STP/kg x 10^4	Δ(Ne) %	Δ'(He) %
p*	3	35.62	17.90	3.991[a]	6.9	1.577	2.7	3.7
c	4	35.62	17.90	-----	---	-----	---	---
p	204	35.39	14.65	4.111[a]	9.2	1.649	4.9	3.3
p	484	34.81	10.66	4.041	5.9	1.695	4.4	0.4
c	866	34.43	6.09	-----	---	-----	---	---
p	1043	34.44	4.20	4.198	7.3	1.762	2.9	3.7
p	1667	34.54	2.70	4.218	7.2	1.780	2.7	3.8
c	1737	34.59	2.50	-----	---	-----	---	---
p	1838	34.63	2.27	4.379	11.2	1.807	4.0	6.2
p	1945	34.64	2.15	4.499[a]	14.2	1.812	4.1	8.9
p	2773	34.68	1.66	4.369	10.7	1.778	1.7	8.4
p	3212	34.72	1.51	4.340[a]	9.9	1.833	4.8	3.8
c	3335	34.76	1.36	-----	----	-----	---	---

... continued

TABLE II. - continued

He-Ne DATA FROM NOVA EXPEDITION, STATION ARGO VI-2;

31.0°S, 177.0°W, 24 September, 1967.

Sampler	Depth (m)	Salinity ‰	Potential Temp. (°C)	He Content cc STP/kg x 10^5	Δ(He) %	Ne Content cc STP/kg x 10^4	Δ(Ne) %	Δ'(He) %
p	3578	34.68	1.55	4.383	11.0	1.878	7.4	1.6
C	3965	34.73	0.89	-----	----	-----	---	---
c	4320	34.72	0.81	-----	----	-----	---	---
p	4423	34.68	1.53	4.442	12.5	1.855	6.0	4.8
p	5307	34.72	0.62	4.273	7.7	1.777	0.8	6.7
c	6287	-----	0.57	-----	----	-----	---	---
p	6291	34.71	0.57	4.404[a]	11.0	1.837	4.1	5.8
c	7268	34.70	0.57	-----	----	-----	---	---
p	7274	34.70	0.57	4.215	6.2	1.838	4.1	0.9
C	8250	34.71	0.56	-----	----	-----	---	---
p	8746***	34.71	0.07	4.337	9.0	1.830	3.2	4.9
	Errors			±0.6%	±1.1**	±0.5%	±1.0**	±1.5

* p - piggyback (~17ml); c - cylinder (~300 ml); C - cylinder (~500 ml).
** The error includes the 0.5% uncertainty in solubility values.
***Sampler post or pre-tripped during sampling, thus Δ'(He) is uncertain.
a He contents with superscript 'a' have an error of ±1.2%.

TABLE III. He-Ne DATA FROM GEOSECS TEST STATION (28° 29' N, 121° 38' W), September, 1969.

Sampler	Depth (m)	Salinity ‰	Potential Temp. (°C)	He Content cc STP/kg x 10^5	Δ(He) %	Ne Content cc STP/kg x 10^4	Δ(Ne) %	Δ'(He) %
c	2	33.71	19.80	4.065	+ 8.2	1.610	+5.0	+2.3
c	208	33.86	9.75	4.073	+ 5.9	1.696	+3.2	+2.0
c	521	34.28	5.92	4.223	+ 8.6	1.742	+3.1	+4.7
p	531	34.23	5.88	3.981	+ 2.3	1.667	-1.4	+4.1
c	927	34.49	4.25	4.480	+14.6	1.825	+6.7	+6.1
p	1521	34.57	2.69	4.437	+12.8	1.828	+5.5	+5.8
c	1955	34.61	2.03	4.430	+12.4	1.835	+5.3	+5.6
p	1965	34.64	2.02	4.384	+11.2	1.829	+5.0	+4.8
p	2245	34.64	1.76	4.429	+12.2	1.849	+6.0	+4.6
C	2490	34.66	1.61	4.467	+13.1	1.815	+3.8	+8.3
p	2501	34.65	1.60	4.606	+16.6	1.905	+9.0	+5.1
p	2740	34.66	1.49	4.521	+14.4	1.825	+4.3	+8.9
c	2986	34.67	1.39	4.539	+14.8	1.839	+5.0	+8.4
p	2996	34.67	1.39	4.523	+14.4	1.888	+7.8	+4.4
C	3496	34.67	1.29	4.468	+13.0	1.827	+4.2	+7.6
p	3898	34.70	1.21	4.373	+10.5	1.878	+7.6	+0.8
c	4100	34.69	1.20	4.393	+11.1	1.868	+6.5	+2.8
p	4111	34.67	1.15	4.439	+12.2	1.868	+6.4	+4.0
			Errors	±0.6%	± 1.1	±0.5%	±1.0	±1.5

TABLE IV. He-Ne DATA FROM HUDSON 70 EXPEDITION (42.0°S, 46.0°W), January, 1970.

Sampler	Depth (m)	Salinity ‰	Potential Temp. (°C)	He Content cc STP/kg x 10^5	Δ(He) %	Ne Content cc STP/kg x 10^4	Δ(Ne) %	Δ'(He) %
c	489	34.19	4.22	4.929	25.9	1.894	10.5	-----
c	988	34.31	2.67	4.766	21.0	1.881	8.4	-----
c	1980	34.80	2.61	4.635	18.0	1.927	11.3	-----
c	2478	34.85	2.50	4.411	12.3	1.860	7.4	2.9
c	2976	34.82	1.94	4.432[a]	12.5	1.935	11.1	- 1.6
c	3475	34.73	0.98	4.467	12.8	1.981	12.7	- 3.5
c	3974	34.68	0.16	4.296	8.1	1.922	8.5	- 2.8
c	4473	34.68	-0.09	4.327	8.7	1.948	9.7	- 3.8
c	4748	34.67	-0.15	4.069	2.2	1.954	10.0	-10.7
			Errors	±0.6%	± 1.1	±0.6%	± 1.1	± 1.6

a. ±0.9%

TABLE V. He-Ne DATA FROM SCAN EXPEDITION (EAST PACIFIC RISE), February, 1970.

Sampler	Location	Depth (m)	Salinity ‰	Potential Temp. (°C)	He Content cc STP/kg x 10^5	Δ(He) %	Ne Content cc STP/kg x 10^4	Δ(Ne) %	Δ'(He) %
c	Station 35, 7.0°S, 103.0°W	1091	34.57	4.01	4.424[a]	13.1	1.793	4.7	7.2[a]
C		2847	34.68	1.56	4.539[b]	14.9	1.788	2.2	12.1[b]
c		4019	34.68	1.45	4.402[a]	11.4	1.783	1.8	9.1[a]
c	Station 38, 6.5°S, 107.0°W	1011	34.57	4.12	4.252[b]	8.8	1.753	2.4	5.8[b]
c		2573	34.68	1.73	4.538[b]	15.0	1.761	0.9	13.9[b]
c		2914	34.70	1.57	4.526[a]	14.6	1.829	4.6	8.7[a]
c	Station 41, 6.0°S, 110.0°W	940	34.56	4.52	4.259[a]	9.1	1.751	2.6	5.8[a]
C		2493	34.68	1.68	4.373[a]	10.8	1.811	3.7	6.1[a]
c		3518	34.70	1.28	4.342[a]	9.8	1.804	2.9	6.1[a]
d*	Station 56, 8.5°N, 113.0°W	2096	34.66	1.89	4.530[b]	14.9	1.831	5.0	8.5[b]
d		3099	34.69	1.38	4.415[b]	11.7	2.008	14.6	-7.0[b]
d		3908	34.69	1.21	4.367[b]	10.4	1.889	7.7	0.6[b]
		Errors			a. ±0.5%	±1.0	±0.5%	±1.0	a. ±1.1
					b. ±1.9%	±2.4			b. ±2.1

*Stainless steel sampler (Dragon flask) of volume ~50 ml.

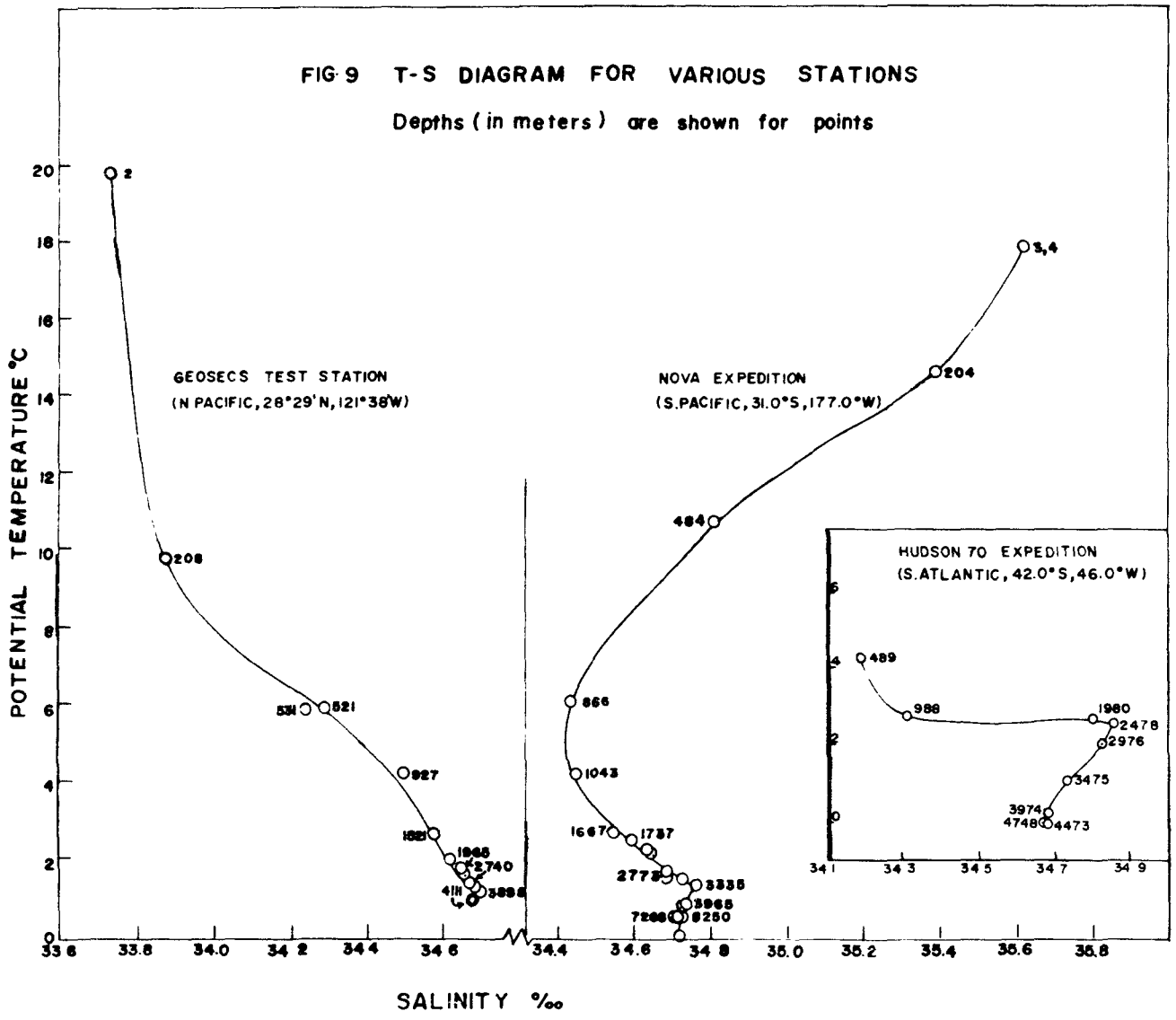
FIG 9 T-S DIAGRAM FOR VARIOUS STATIONS
Depths (in meters) are shown for points
GEOSECS TEST STATION
(N PACIFIC, 28°29'N, 121°38'W)
NOVA EXPEDITION
(S.PACIFIC, 31.0°S, 177.0°W)
HUDSON 70 EXPEDITION
(S.ATLANTIC, 42.0°S, 46.0°W)
POTENTIAL TEMPERATURE °C
SALINITY ‰
2
208
521
927
1965
2740
3898
204
484
866
1043
1667
1787
2773
3335
5965
6250
489
988
1980
2478
2976
3475
3974
4748
4473

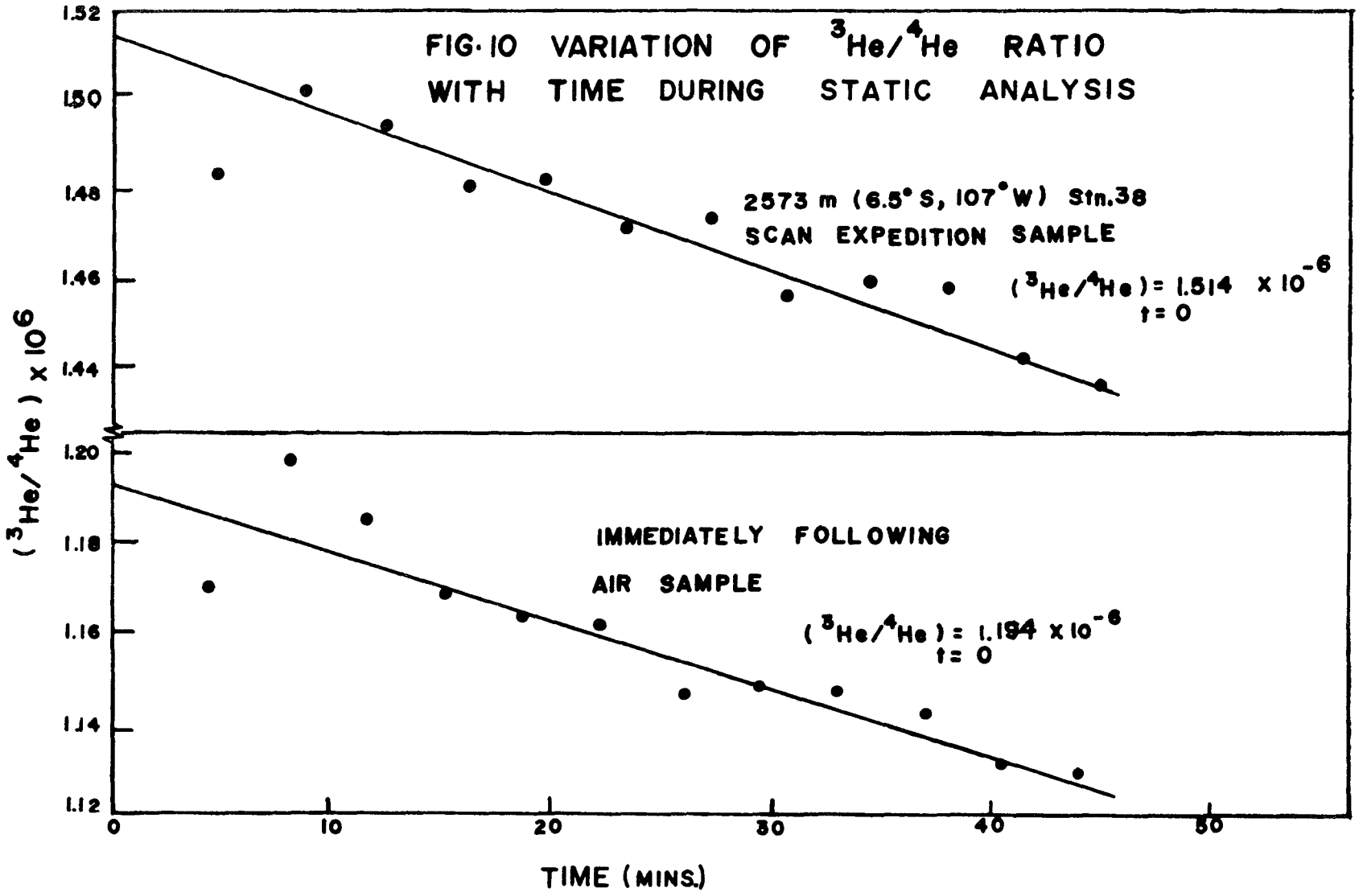
FIG·10 VARIATION OF $^3He/^4He$ RATIO WITH TIME DURING STATIC ANALYSIS
2573 m (6.5° S, 107° W) Stn.38
SCAN EXPEDITION SAMPLE
$(^3He/^4He) = 1.514 \times 10^{-6}$
t = 0
IMMEDIATELY FOLLOWING
AIR SAMPLE
$(^3He/^4He) = 1.194 \times 10^{-6}$
t = 0
$(^3He/^4He) \times 10^6$
TIME (MINS.)
1.52
1.50
1.48
1.46
1.44
1.20
1.18
1.16
1.14
1.12
0
10
20
30
40
50

$(^3He/^4He)_{t=o}$ ratios of the air standards were quite reproducible from day to day for a particular series of analyses where instrument settings were unchanged, therefore their grand average was used in order to calculate $\delta(^3He)$ according to equation (2). However, the air value varied from series to series, because of changes in instrument settings.

Since the saturation anomaly Δ (see equation (1)) is the proper quantity for flux computations, a relationship for $\Delta(^3He)$ can be obtained from the definitions of Δ and α, where α is the isotopic fractionation factor for ^3He and ^4He, i.e., $\alpha = \frac{\beta(^3He)}{\beta(^4He)}$ (18). The equation for $\Delta(^3He)$ is as follows:

$$\Delta(^3He)\ \% = [\delta_3 + \Delta_4 + 10^{-2}\ \delta_3\Delta_4 - 10^2(\alpha-1)]\alpha^{-1}, \text{ - - - - } (9)$$

where $\delta_3 \equiv \delta(^3He)$, $\Delta_4 \equiv \Delta(^4He)$, and $(\alpha-1)$ is the helium isotope solubility effect (18). The derivation of equation (9) is given in Appendix A.

The results for $\delta(^3He)$, $\Delta'(He)$ and $\Delta'(^3He)$ are cited in Tables VI to IX. $\Delta'(^3He)$, the additional (primordial) component of ^3He, calculated by substituting Δ'_4 for Δ_4 in equation (9), is also listed in the tables. The $\delta(^3He)$ and

TABLE VI. ^{3}He-^{4}He DATA FROM NOVA EXPEDITION, STATION ARGO VI-2; 31.0°S, 177.0°W, September, 1967.

Sampler	Depth (m)	Δ(He) %	Δ'(He) %	δ(^{3}He)** %	Δ'(^{3}He) %
P	3	6.9	3.7	--------	--------
c	4	-----	(3.7)*	-1.8±2.2	3.2±2.7
p	204	9.2	3.3	--------	--------
p	484	5.9	0.4	--------	--------
c	866	-----	(1.4)	1.5±2.1	4.2±2.7
p	1043	7.3	3.7	--------	--------
p	1667	7.2	3.8	--------	--------
c	1737	-----	(6.7)	21.8±2.1	31.5±2.7
p	1838	11.2	6.2	--------	--------
p	1945	14.2	8.9	--------	--------
p	2773	10.7	8.4	--------	--------
p	3212	9.9	3.8	--------	--------
c	3335	-----	(3.1)	5.8±1.9	10.4±2.4
p	3578	11.0	1.6	--------	--------
C	3965	-----	(2.5)	10.1±1.8	14.2±2.4
c	4320	-----	(4.4)	10.8±2.1	17.0±2.7
p	4423	12.5	4.8	--------	--------
p	5307	7.7	6.7	--------	--------

continued ...

TABLE VI - continued

Sampler	Depth (m)	Δ(He) %	Δ'(He) %	δ(^{3}He)** %	Δ'(^{3}He) %
c	6287	-----	(5.8)	7.8±1.9	15.4±2.4
p	6291	11.0	5.8	--------	--------
c	7268	-----	(0.9)	12.2±2.0	14.6±2.7
p	7274	6.2	0.9	--------	--------
C	8250	-----	-----	8.4±1.9	--------
p	8746	9.0	4.9***	--------	--------
Errors		±1.1	±1.5	--------	--------

* Bracketted Δ'(He) values are interpolated from the Δ'(He) vs. depth graph shown in Fig. 11.

** Published data [Clarke, Beg, and Craig (16)].

*** Not used for interpolation (see footnote ***, Table II).

TABLE VII. ^{3}He-^{4}He DATA FROM GEOSECS TEST STATION (28° 29' N, 121° 38' W), September, 1969.

Sampler	Depth (m)	Δ(He) %	Δ'(He) %	δ(^{3}He)* %	Δ'(^{3}He) %
c	2	8.2	2.3	1.5±1.7***	-------
c	208	5.9	2.0	8.0±2.2***	-------
c	521	8.6	4.7	8.5±1.5	15.0±2.1
p	531	2.3	4.1	(8.8±2.0)**	-------
c	927	14.6	6.1	18.3±1.5	27.1±2.2
p	1521	12.8	5.8	(20.4±2.0)	-------
c	1955	12.4	5.6	21.9±1.7	30.3±2.3
p	1965	11.2	4.8	(21.9±2.0)	-------
p	2245	12.2	4.6	(21.9±2.0)	-------
C	2490	13.1	8.3	21.9±1.5	33.6±2.2
p	2501	16.6	5.1	(21.8±2.0)	-------
p	2740	14.4	8.9	(20.7±2.0)	-------
c	2986	14.8	8.4	19.5±1.6	31.3±2.2
p	2996	14.4	4.4	(19.5±2.0)	-------
C	3496	13.0	7.6	16.5±1.5	26.8±2.1
p	3898	10.5	0.8	(14.0±2.0)	-------
c	4100	11.1	2.8	12.8±2.0	17.3±2.5
p	4111	12.2	4.0	(12.7±2.0)	-------
Errors		±1.1	±1.5	---------	--------

continued ...

TABLE VII - continued

* Published data [Clarke, Beg and Craig (17)].

** The bracketted $\delta(^3He)$ values are interpolated from the graph of $\delta(^3He)$ vs. depth (see Fig. 12).

*** Correction for tritium decay in the samples during storage before gas extraction amounts to 1% (17). Therefore $\delta(^3He) = 0.5\%$ is plotted in Fig. 15. The 208 m sample data was not used in Fig. 15 because of large uncertainty in the estimate of tritium correction (17).

TABLE VIII. ^{3}He-^{4}He DATA FROM HUDSON 70 EXPEDITION (42.0°S, 46.0°W), January, 1970.

Sampler	Depth (m)	Δ(He) %	Δ'(He) %	$\left(\frac{^{3}He}{^{4}He}\right)^{*}_{t=o} \times 10^{6}$	δ(^{3}He) %	Δ'(^{3}He) %
c	489	25.9	-----	1.175±.005	-2.1±0.7	-------
c	988	21.0	-----	1.198±.005	-0.3±0.7	-------
c	1980	18.0	-----	1.269±.007	5.7±0.9	-------
c	2478	12.3	+ 2.9	1.251±.007	4.2±0.9	8.5±1.9
c	2976	12.5	- 1.6	1.229±.027	4.6±3.4	4.2±3.8
c	3475	12.8	- 3.5	1.255±.006	4.5±0.8	2.0±1.9
c	3974	8.1	- 2.8	1.262±.002	5.1±0.4	3.4±1.7
c	4473	8.7	- 3.8	1.280±.011	6.5±1.2	3.6±2.0
c	4748	2.2	-10.7	1.271±.008	5.8±1.0	-4.3±1.9
Errors		±1.1	± 1.6			
Atmospheric value for this series				1.201±.003		

* Observed ratios, uncorrected for instrumental discrimination factor.

TABLE IX. ^{3}He-^{4}He DATA FROM SCAN EXPEDITION (EAST PACIFIC RISE), February, 1970.

Sampler	Location	Depth (m)	Δ(He) %	Δ'(He) %	$\left(\frac{^{3}He}{^{4}He}\right)^{*}_{t=o} \times 10^{6}$	$\delta(^{3}He)$ %	$\Delta'(^{3}He)$ %
c	Station 35, 7.0°S, 103.0°W	1091	13.1	7.2±1.1	1.407±.007	16.5±0.8	26.4±1.4
C		2847	14.9	12.1±2.1	1.574±.006	30.3±1.8	47.8±2.8
c		4019	11.4	9.1±1.1	1.517±.008	25.6±1.0	38.7±1.5
c	Station 38, 6.5°S, 107.0°W	1011	8.8	5.8±2.1	1.424±.006	17.9±0.8	26.3±2.3
c		2573	15.0	13.9±2.1	1.514±.003	25.4±0.6	44.6±2.3
c		2914	14.6	8.7±1.1	1.581±.006	31.0±0.8	44.1±1.4
c	Station 41, 6.0°S, 110.0°W	940	9.1	5.8±1.1	1.396±.005	15.6±0.7	23.8±1.4
C		2493	10.8	6.1±1.1	1.608±.006	33.2±0.8	43.0±1.4
c		3518	9.8	6.1±1.1	1.478±.006	22.4±0.8	31.4±1.4
d	Station 56, 8.5°N, 113.0°W	2096	14.9	8.5±2.1	1.660±.010	33.5±2.2	46.6±3.0
d		3099	11.7	-7.0±2.1	1.552±.016	24.8±2.6	17.3±3.3
d		3908	10.4	0.6±2.1	1.568±.020	26.1±3.0	28.4±3.7
Atmospheric value for stations 35, 38 and 41					1.208±.004		
Atmospheric value for station 56					1.244±.017		

* Observed ratios, uncorrected for instrumental discrimination factor.

total He-Ne measurements for NOVA and GEOSECS stations were not done on the same water samples. Therefore, $\Delta'(He)$ values corresponding to the published $\delta(^3He)$ data (16) for the NOVA station were interpolated from a graph of the measured $\Delta'(He)$ versus depth shown in Fig. 11. They are written within brackets in the fourth column of Table VI. The same procedure was adopted for the non-measured $\Delta'(He)$ data (in Table VII) of the GEOSECS station with the difference that $\delta(^3He)$ data (17) was plotted against depth as shown in Fig. 12. This is justified since the GEOSECS profile yields a broad maximum at mid-depth consisting of four points compared to a single point at 1737 m for the NOVA station.

The $(^3He/^4He)_{t=o}$ values for HUDSON and SCAN expeditions are also presented in Tables VIII and IX respectively. Atmospheric $(^3He/^4He)_{t=o}$ is quoted in each case for comparison. The $\Delta'(He)$ and $\Delta'(^3He)$ values for the first three (<2000 m) HUDSON samples are not computed because of unexpectedly high $\Delta(He)$ observed for them (25.9, 21.0 and 18.0 %). These values are not understood at present. It seems possible that either the analyses were wrong or something happened during sampling. In any case, the results are not considered reliable and have not been plotted in Fig. 13, (also Fig. 15), which shows the $\delta(^3He)$ % and $\Delta'(He)$ % profiles versus depth. Similar plots for the

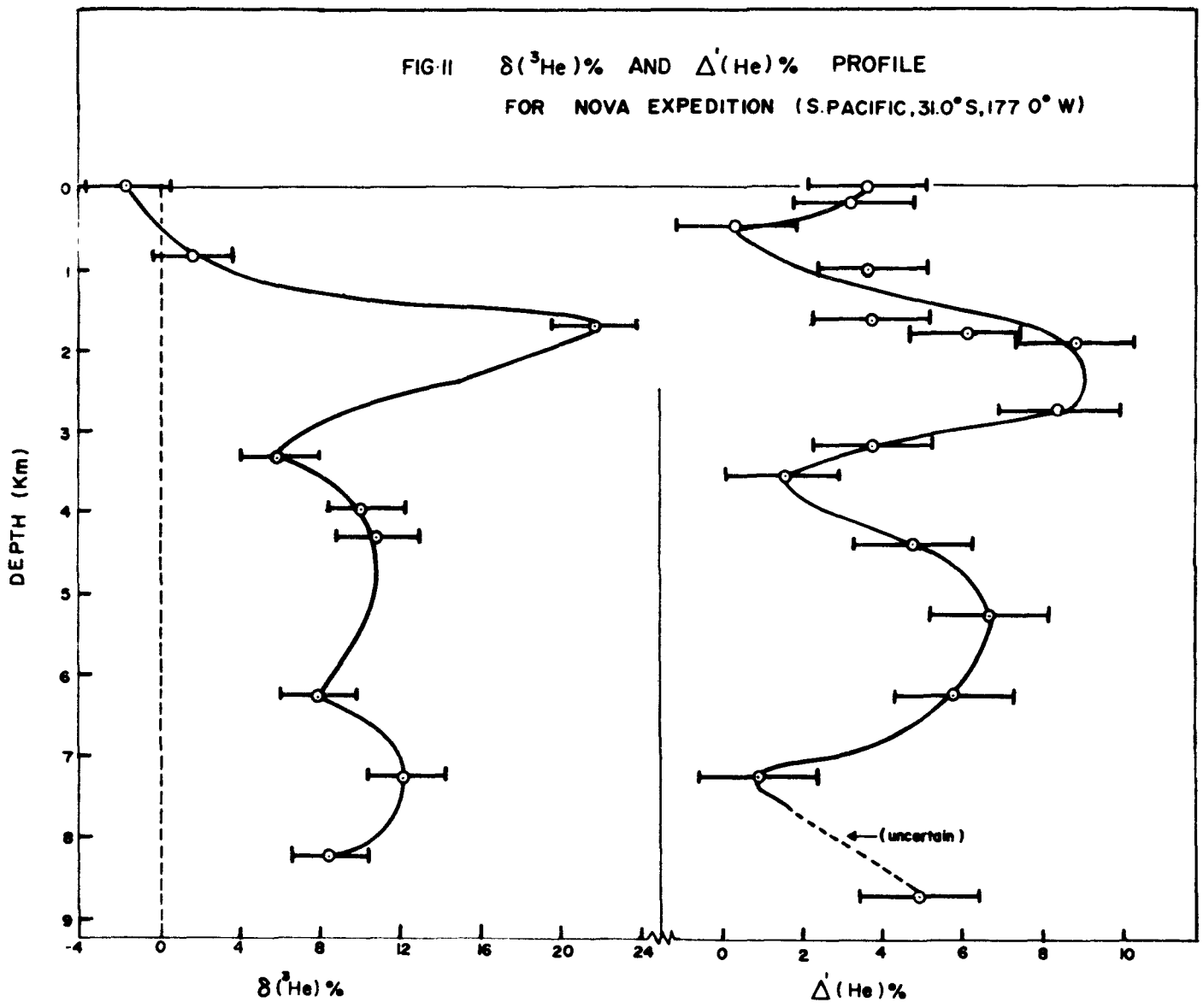
FIG·11 δ(³He)% AND Δ'(He)% PROFILE
FOR NOVA EXPEDITION (S.PACIFIC, 31.0°S, 177 0° W)
DEPTH (Km)
0
1
2
3
4
5
6
7
8
9
-4
0
4
8
12
16
20
24
δ(³He)%
0
2
4
6
8
10
Δ'(He)%
(uncertain)

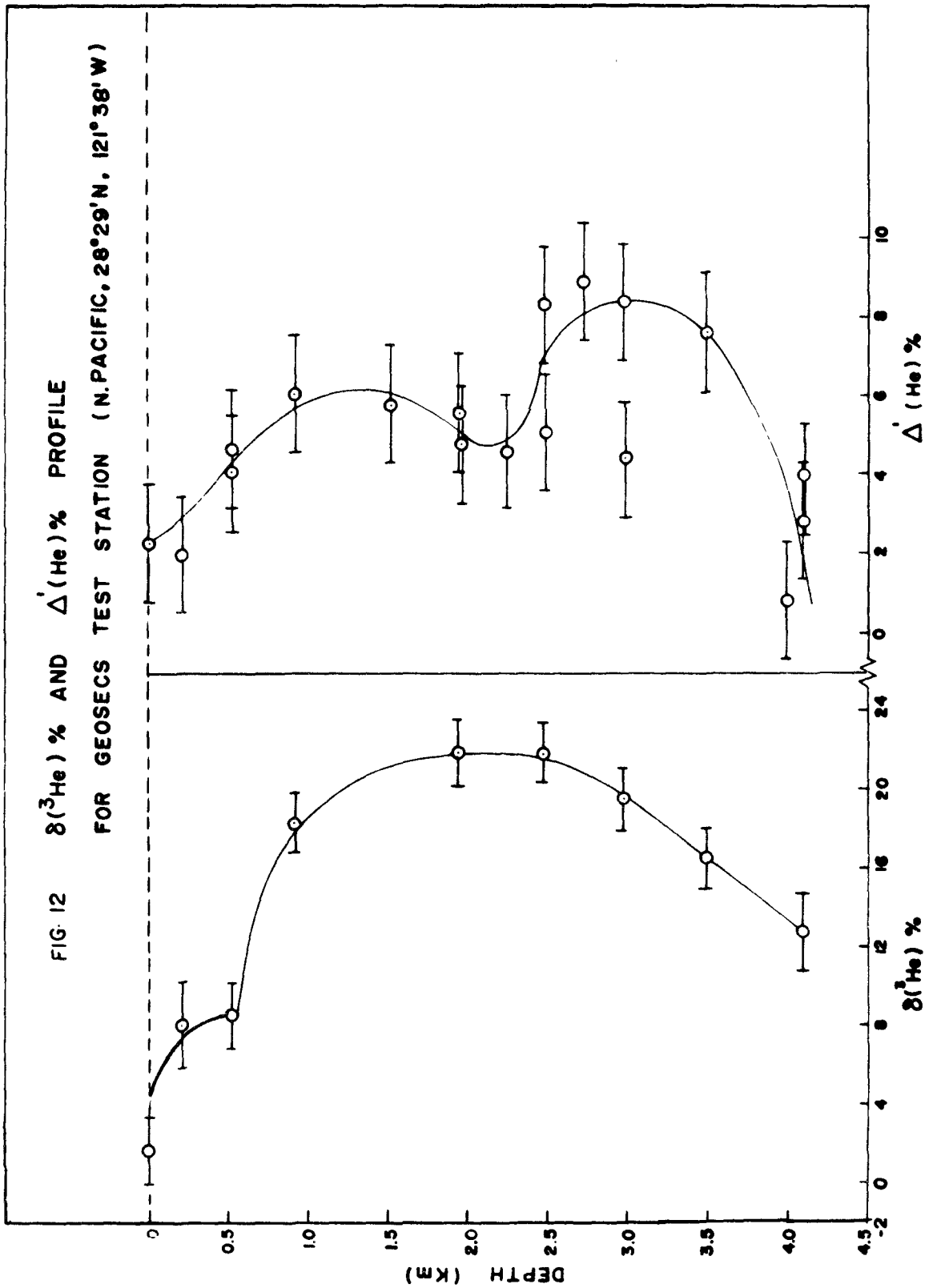
FIG. 12 δ(³He)% AND Δ'(He)% PROFILE
FOR GEOSECS TEST STATION (N.PACIFIC, 28°29'N, 121°38'W)
DEPTH (KM)
0
0.5
1.0
1.5
2.0
2.5
3.0
3.5
4.0
4.5
δ(³He) %
-2
0
4
8
12
16
20
24
Δ'(He) %
0
2
4
6
8
10

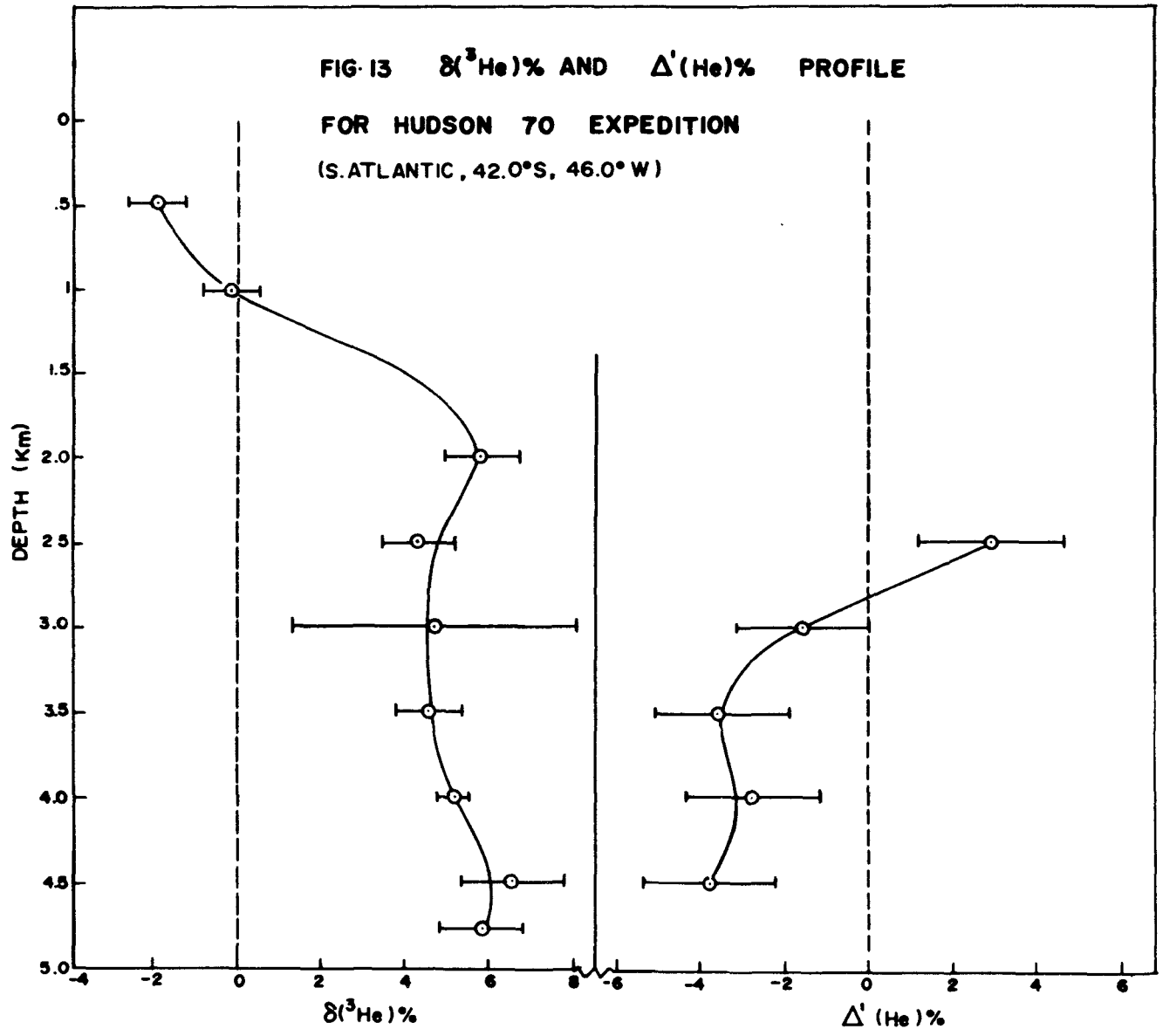
FIG· 13 δ(³He)% AND Δ'(He)% PROFILE
FOR HUDSON 70 EXPEDITION
(S. ATLANTIC, 42.0°S, 46.0° W)
DEPTH (Km)
0
.5
1
1.5
2.0
2.5
3.0
3.5
4.0
4.5
5.0
-4
-2
0
2
4
6
8
δ(³He)%
-6
-4
-2
0
2
4
6
Δ' (He)%

SCAN expedition stations 35, 38 and 41 are given in Fig. 14; the curves merely represent the probable trend at these locations since only three samples per station were available for analysis. The facts that (i) samplers used for station 56 could not be leak-tested prior to water sampling; (ii) their Δ'(He) data scatter badly from negative to positive values, render the station 56 data unreliable. Hence they are excluded from Figures 14 and 15.

C. $\delta(^3He)$ AND Δ'(He) CORRELATION

As mentioned in Chapter I, a weak correlation between $\delta(^3He)$ and Δ(He) was observed in our previous measurements (16) but firm conclusions could not be made at that time because the Δ(He) data were of insufficient precision. During the present analyses, the use of the isotope dilution method has given much more accurate results for He-Ne contents and hence Δ(He) and Δ(Ne), thus making it possible to re-examine the correlation problem.

Artificial tritium decay does not contribute appreciably to the $\delta(^3He)$ observed for waters deeper than 500 m (27), and the ^3He excess is assumed to be mainly of

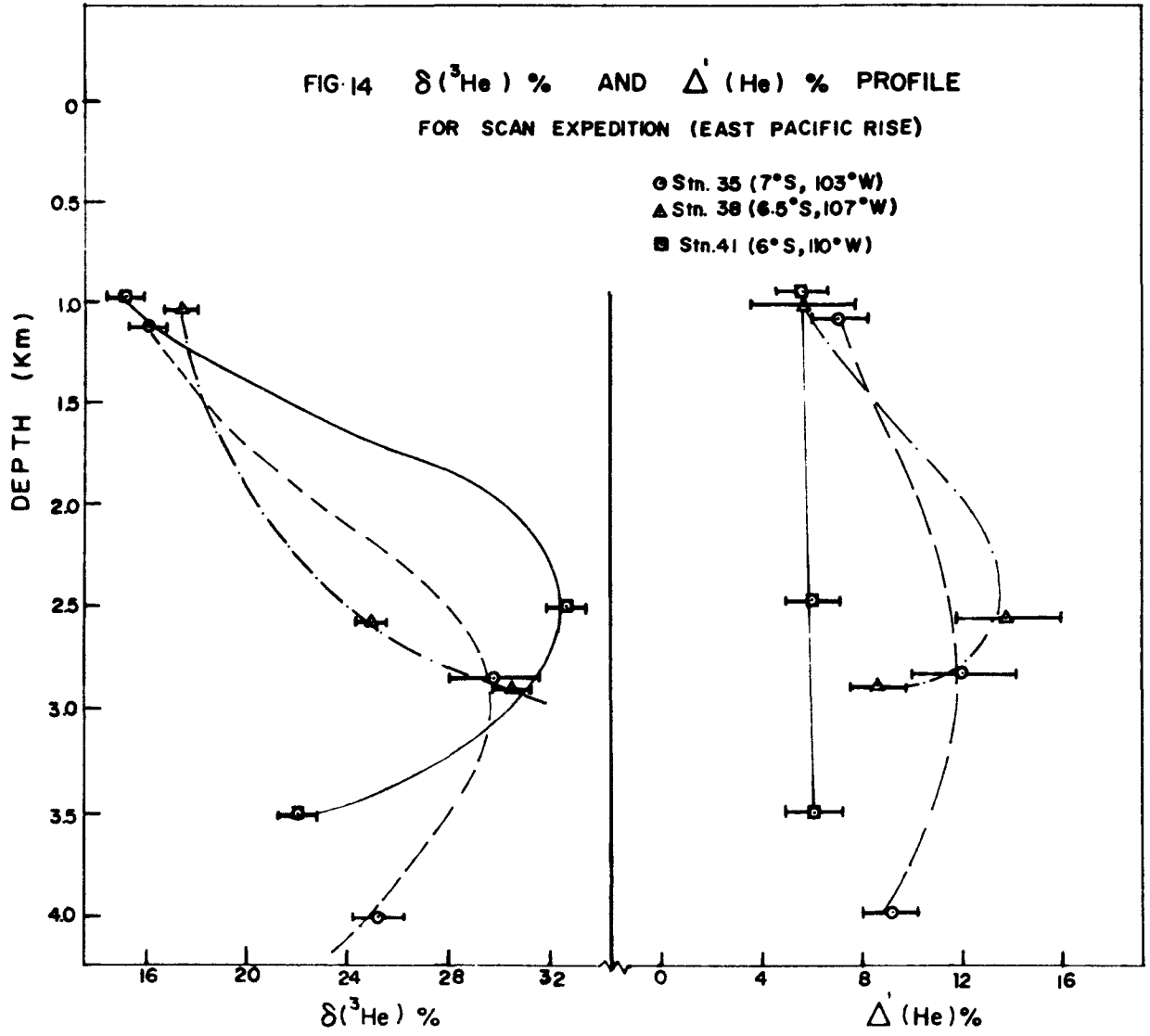
FIG·14 δ(³He) % AND Δ'(He) % PROFILE
FOR SCAN EXPEDITION (EAST PACIFIC RISE)
Stn. 35 (7°S, 103°W)
Stn. 38 (6.5°S, 107°W)
Stn.41 (6°S, 110°W)
DEPTH (Km)
0
0.5
1.0
1.5
2.0
2.5
3.0
3.5
4.0
16
20
24
28
32
δ(³He) %
0
4
8
12
16
Δ'(He)%

primordial origin (16,17,28), therefore Δ'(He) [i.e. primordial and radiogenic components] and not the Δ(He) is the proper quantity to compare with $\delta(^3He)$ to search for a possible correlation. The surface $\delta(^3He)$ values when corrected in the appropriate way for tritium decay can also be used for this purpose.

This has been done for the Pacific ocean data from the GEOSECS (17 points), NOVA (8 points), and SCAN (9 points) expeditions and the result is shown in Fig. 15. The HUDSON '70 data is excluded from this diagram because they belong to a different ocean (Atlantic) and are less reliable (see Section B). Treating the $\delta(^3He)$ and Δ'(He) values as pairs of measurements, with equal uncertainty, and assuming a linear relationship of the form,

$$\delta(^3He) = a + b\ \Delta'(He),$$

the coefficient of linear-correlation r was found to be equal to 0.677 for 34 data points. A check made for the probability $P_c(r,N)$, that a random sample of 34 uncorrelated experimental points would yield a linear-correlation coefficient as large as or larger than the observed value of $|r|$, gave

$$P_c(0.677,\ 34) < 0.001.$$

Thus the probability of correlation is very high and the assumed fit to a straight line equation seems valid.

The least squares fit analysis was carried out by weighting the data variables equally, and the values of a, b and their errors (one standard deviation) were determined. In this way, the following equation was obtained:

$$\delta(^3He) = (5.60 \pm 2.39) + (1.97 \pm 0.38)\ \Delta'(He);- - - - \quad (10)$$

It is shown in Fig. 15 by the solid line. When the data is weighted according to analytical errors (properly treated for their uncorrelation to each other (29)), the value of the intercept 'a' is reduced from (5.60 $\pm$ 2.39) to (5.19 $\pm$ 1.47). This relationship is represented by a dashed line in Fig. 15. Similarly, a fit to a quadratic equation did not yield a reliable relationship because of large scatter of the data (especially the SCAN values) due to non-uniform sampling as regards depth for the various stations. Therefore, both of these treatments have been overlooked, for the present, in favour of the simple relationship described by the equation (10). Further discussions about the significance and implications of equation (10) are deferred to Chapter IV.

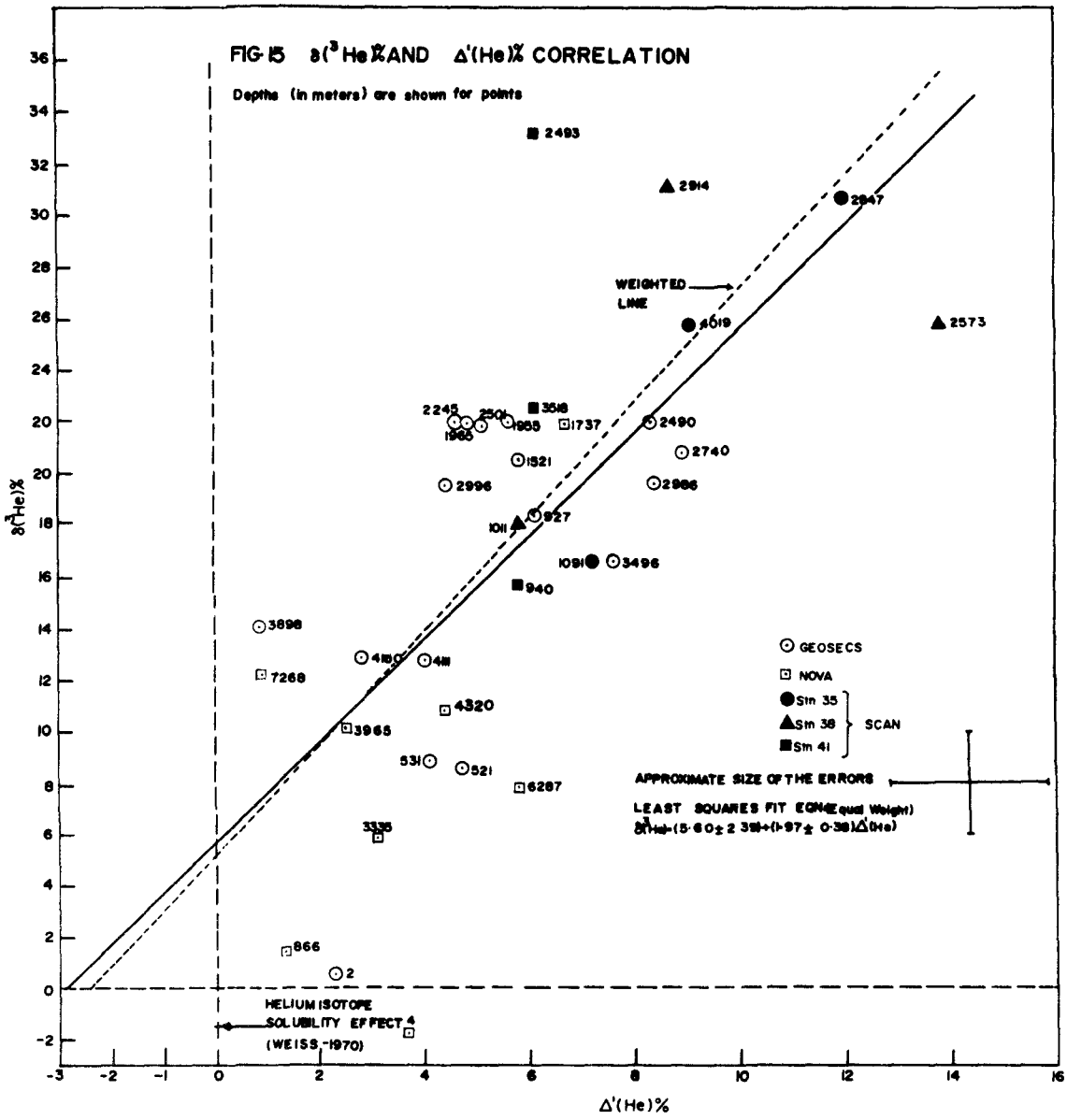
FIG-15 δ(³He)% AND Δ'(He)% CORRELATION
Depths (in meters) are shown for points
2493
2914
2947
WEIGHTED LINE
2619
2573
2245
2501
3518
1965
1737
2490
1965
2740
1521
2996
2986
1011
927
1091
3496
940
3898
4180
411
7268
4320
3965
531
521
6287
3336
866
2
HELIUM ISOTOPE SOLUBILITY EFFECT
(WEISS-1970)
GEOSECS
NOVA
Stn 35
Stn 38
Stn 41
SCAN
APPROXIMATE SIZE OF THE ERRORS
LEAST SQUARES FIT EQN (Equal Weight)
δ(³He)=(5·60±2 38)+(1·97± 0·38)Δ'(He)
δ(³He)%
Δ'(He)%

CHAPTER IV

DISCUSSION

A. DISCUSSION OF THE RESULTS

1. ^{3}He Results

(a) General Features

The combined $\delta(^3He)$ data from all the stations range between (-2.1 ± 0.7) to (33.5 ± 2.2) % with lower values in the Atlantic ocean relative to the Pacific ocean by roughly a factor of four. These results are in good agreement with earlier measurements reported from this laboratory (16,17), which were the first measurements ever performed for oceanic ^{3}He. The confidence in ^{3}He results is achieved because of:

(i) Careful leak tests of the sample containers prior to water sampling and subsequent negligible blanks (<0.1%) observed for the extraction and sample introduction systems.

(ii) He-Ne results obtained from the small splits of the same water samples by isotope dilution, agree well with the data obtained in other laboratories

(11,14,15) in spite of the fact that different sampling techniques were employed.

All ^3He results in general show a definite trend with the sampling depths as is obvious from Figs. 11-14; this trend is summarized below.

Depth Interval (m)	Range of Values for $\delta(^3He)$ (‰)
0 - 1000	-2.1 to 18.3
1000 - 4000	4.2 to 33.2
below 4000	5.8 to 12.7

In both the Atlantic and Pacific oceans a "mid-depth" $\delta(^3He)$ maximum (5.1‰ and 21.8 - 33.2‰ respectively) is observed.

The He^3/He^4 ratio in surface waters should approximately be the same as that of the atmosphere. But, as mentioned in Chapter I, $\delta(^3He)$ variations from zero can result from bomb-produced tritium decay and because of the ^3He solubility effect (18). However, the tritium correction is applicable only to the GEOSECS ^3He data where large ^3H contents have been measured (27) for surface waters. NOVA samples do not require such a correction as the surface ^3H values at this latitude (31°S) are at least a factor of 10 lower than the values at the GEOSECS

location (28° 29' N)(30). For samples obtained from the remaining two expeditions, no ^{3}H correction is necessary due to the lack of surface samples.

(b) NOVA (S. Pacific) and GEOSECS (N. Pacific) ^{3}He Data

The NOVA and GEOSECS ^{3}He data have been compared and discussed elsewhere (16,17,28). However, some additional features are described here. In the NOVA T-S profile (Kermadec Trench) given in Fig. 9, two water cores entering below the surface layer are recognizable; Antarctic Intermediate Water (AAI) marked by the salinity minimum at 900m and the South Pacific Central Water (SPC) exhibiting a salinity maximum at 3500m. Below 3500 m, the trench water is isohaline but stratified according to temperature. The T-S data from both the stations compare well with the data reported in the literature (26,31,32) for locations close to the present one.

The pronounced NOVA ^{3}He maximum occurs at about 1737m between the two salinity extrema; the mid-depth smooth T-S contour signifies a well mixed layer and would appear to suggest a broader $\delta(^{3}He)$ vs. depth profile, had more samples been obtained at these depths. The fact that equal values for $\delta(^{3}He)$ have been measured at mid-depths for both the GEOSECS and NOVA stations, indicates

that these depths of the N. Pacific ocean are filled by water of the same character as that found in the northern portion of the S. Pacific. Also, it is interesting to note that the T-S profiles at the two locations are similar (see Fig. 9), between 1 - 4 km.

(c) HUDSON '70 (S. Atlantic) ^{3}He Data

The T-S profile for this station, well supported by others (33), indicates three cores of water masses mixing together. A less saline cold water (AAI), a more saline cold N. Atlantic Deep Water (NAD), and very cold Antarctic Bottom Water (AAB). Because of being fed by the waters from the Antarctic, the S.Atlantic water is relatively young. Indeed, extensive studies of ^{14}C in ocean water (34) have shown that most of the water in the N. Atlantic below 600 m persists as deep water for 650 years on average, while water masses originating in the Antarctic have residence times of about half that period. Thus an age of ~300 years can be assumed for the S. Atlantic deep waters, which is about one third of the age of the S. Pacific waters (5). Hence $\delta(^{3}He)$ values might be expected to reflect this age difference in the two oceans. In fact, the present results do indicate $\delta(^{3}He)$ values three times higher in the S. Pacific ocean

in contrast to the values observed for the S. Atlantic ocean. Thus the hypothesis of ^3He leaking from a source inside the oceans and enriching the water according to its age seems very convincing, in a semi-quantitative way.

(d) SCAN (East Pacific Rise) ^3He Data

The SCAN samples are of special interest because of the following reasons:

(i) A large excess of oceanic ^3He is observed from all the four stations over the East Pacific Rise (EPR), even though the Station 56 data is less reliable.

(ii) These stations are located near the high heat flow areas (35) connected with volcanic and tectonic activity. In this regard, the ^3He data seem to indicate that a major source of ^3He is located somewhere near these sampling stations.

Only three water samples per station were available for analysis, one each from the intermediate, deep and bottom waters, at the Stations 35, 38 and 41. At Station 56, even the intermediate depth sample is missing. It is unfortunate that so few samples were procured.

As mentioned above, all the four stations lie

near a zone of anomalously large heat flow from the ocean floor. According to the bathymetric chart as well as the deepest sample (which represents the ocean bottom), Station 38 lies on the crest of EPR; the location of other stations can be seen in Fig. 8. The heat flow values, approximated from the data compiled by Bullard (36), are given below.

Station No.	Bottom Depth (m)	Heat Flow (μ Cal/cm^2 sec)
35	4019	~2.0
38	2914	~7.95
41	3518	~7.95
56	3908	~0.93
Mean Oceanic Value (away from ridges)		1.08

Because of the high heat flow, the deep water (>2400m) temperatures at Station 38 are slightly higher than those recorded at other stations (see Table V). Bottom water salinities of Stations 38 and 41 are also higher -- a possible consequence of lava activity. All the stations exhibit maximum ^{3}He values at the mid-depths (see Fig. 14), except Station 38, where an increase in $\delta(^3He)$ values with depth is observed all the way to the bottom. At first glance, this would appear to indicate

that the source of ^3He is at the rise crest, however it should be pointed out that the observation could be interpreted just as well by assuming that the material on the rise does not release ^3He at any unusual rate, but merely serves to truncate the profile in the observed way. Nonetheless, the fact that $\delta(^3He)$ values are higher across the EPR than at other Pacific stations examined to date seems to indicate that these samples were taken closer to a major source of ^3He. Further work is needed to prove whether or not this source is indeed the rise crest.

From a study of the isotherms and isohalines at depths >2000 m across the EPR along 28°S, Warren (31) has observed that on the western flank of the rise isotherms dip downward abruptly as they approach the rise, with no corresponding distortion of the isohalines, indicating heat transfer by conduction. However, on the eastern flank of the rise, no such distortion is observed for either of them, as if convecting mixing were occurring there. Even though Warren's study is inconclusive due to limited data, the ^3He results coupled with this type of information will probably yield some important conclusions in the future.

In summary, the EPR waters are enriched in ^3He by a factor of 1.5 relative to the Pacific waters (cf. NOVA

and GEOSECS) indicating that the sampling was closer to the ^{3}He source. At this stage, no firm conclusions can be made on the basis of the present data.

2. Helium-Neon Results

(a) Pacific Waters

The He-Ne concentrations measured by isotope dilution for the NOVA (S. Pacific), GEOSECS (N. Pacific) and SCAN (E. Pacific Rise) samples are in good agreement with the data reported from other laboratories (6,11,14, 15). Excluding a few points, the values of Δ(He) and Δ(Ne) range between 2 - 16% and 1 - 8% respectively.

A broad Δ(He) peak for mid-depths levelling off near the bottom is demonstrated by the GEOSECS data (Table III); the Δ(Ne) values on the other hand, fluctuate around 6% after passing through a maximum at 2501 m. Therefore a double-peaked Δ'(He) profile shown in Fig. 12 is formed. The He-Ne contents yielded by pairs of samples collected at nearby depths (e.g. 4100 and 4111 m etc.), agree quite well with each other and hence provide a means of checking the results; any small difference in the concentrations of He and Ne in such pairs is probably not real because of the inherent measurement errors. This

implies that the Δ'(He) minimum ~2500 m (Fig. 12) may actually be non-existent and that the true Δ'(He) curve is similar to the $\delta(^3He)$ curve at the N. Pacific station.

The low saturation anomaly found for the 531 m GEOSECS sample, compared to the others, does indicate something wrong with this sample. Actually, such a result can be explained by a small leak in the sampler, which allowed equilibration with the atmosphere at the storage temperature (~20°C). The net changes in Δ for He and Ne with respect to the 521 m sample are 6.3 and 4.5% respectively. These are roughly the changes to be expected if a sample with the He and Ne contents of the 521 m water had equilibrated with the atmosphere at 20°C.

In spite of the fact that the NOVA ^3He and He-Ne data were not obtained from the same water samples, the Δ(He) values do correspond with the $\delta(^3He)$ values exhibiting three maxima at 1945, 4423 and 6291 m (see Table II). Roughly equal values of Δ(Ne) (4%) are observed for the surface and near bottom waters (>5 km) compared to the deep water maximum of ~7%. Upon summation, the Δ(He) and Δ(Ne) profiles yield the Δ'(He) curve with a secondary maximum at 5307 m (see Fig. 11). The low Δ(Ne) values for the bottom trench water show that the amount of air

injection is relatively small. Therefore, the secondary Δ'(He) maximum (~6%) at these depths can be attributed to the radiogenic ^{4}He coming off the ocean bottom and the sides of the trench; the deep water (2000 m) Δ'(He) of ~8% might possibly be the combination of radiogenic and primordial ^{4}He, the later leaking out along with the ^{3}He at the mid-depths. That is, the extra 2% is an upper limit for the primordial ^{4}He contribution to the total Δ(He) measured at mid-depths. Such an idea seems promising but further speculations should be deferred until future investigations substantiate it.

The He-Ne data combined for the four SCAN stations form double-peaked depth profiles which could be smoothed out to one broad peak if the 2493 m value of Δ(He) and 2573, 2847 and 3099 m values of Δ(Ne) (see Table V) are ignored. The He and Ne saturation anomalies are higher, and similar respectively to the NOVA He and Ne values. The individual profiles of Δ'(He) for Station 35, 38 and 41 are shown in Fig. 14, each showing mid-depth maximum.

(b) South Atlantic Waters

The He content of the first three (<2000 m) samples is unexpectedly very high (see Table IV) and does not

correlate with He contents of the Pacific waters at the corresponding depths; the agreement is good, however, for the deeper samples except the 4748 m sample. Examination of the peak height data obtained during the ^3He-^4He measurements has shown that the helium contents measured by isotope dilution are genuine and do not appear to indicate any anomalous behaviour during mass spectrometry. The comparatively low Δ(Ne) values argue against complete or partial dissolution of air bubbles in these waters because in either case the Ne and He saturation anomalies would increase roughly in equal proportions. This strongly suggests that the three samples had undergone preferential He leakage without suffering temperature changes during sampling or extraction procedures. Such an effect would decrease their $\delta(^3He)$ values by ~1% only, thus the $\delta(^3He)$ data is trustworthy.

However, there is a possibility that the samplers pre-tripped; that is, the water was collected at much shallower depths (even surface waters) than recorded, due to some malfunction in the triggering system. But, this idea is not supported by the neon results. It looks as if the ΔHe for the 4748 m sample is smaller by approximately 5% than would be expected. It was collected at -0.15°C and due to a leaky valve in the sample cylinder

it could have partially equilibrated with the atmosphere at ~20°C, which would result in a maximum decrease of 5% for ΔHe.

The mean He and Ne concentrations below 1500 m for both the oceans are listed in Table X. The maxima are also indicated. It can be seen that the S. Atlantic Ne contents are in general higher than those of the Pacific waters, indicating that all the observed He excess in the Atlantic is of atmospheric origin. It is unfortunate that the surface data turned out to be unreliable. On the other hand, about 60% of the He excess observed in the Pacific deep waters is of atmospheric origin. A similar conclusion for the Pacific has been arrived at in a separate study of He-Ne-Ar data (20).

The present investigation has played the part of a general survey in the two oceans, thus demonstrating the necessity of detailed future investigations. Measurements of all the rare gases, as well as tritium, carried out on the same samples cannot be over-emphasized. Wherever possible, duplicate water samples should be procured. Tight sampling, i.e. close spacing between sampling depths, at different locations throughout the various

TABLE X. He-Ne CONCENTRATIONS OF OCEANS BELOW 1500 m.

Ocean	Helium Concentration (cc STP/kg x 10^5) Mean	Helium Concentration (cc STP/kg x 10^5) Maximum	Neon Concentration (cc STP/kg x 10^4) Mean	Neon Concentration (cc STP/kg x 10^4) Maximum
S. Pacific*	4.352	4.499 (1900m)****	1.820	1.878 (3600m)
N. Pacific	4.462	4.606 (2500m)	1.850	1.905 (2500m)
E. Pacific Rise**	4.453	4.538 (2600m)	1.796	1.829 (2900m)
S. Atlantic***	4.387	4.467 (3500m)	1.928	1.981 (3500m)

* The 8746 m sample is excluded.

** Excluding Station 56 data.

*** Excluding the 4748 m sample. The 1980 m He value is also excluded.

**** Approximate depths at which maximum was observed--given in parentheses.

oceanic layers would be of great advantage for comparison purposes. Definitely, the East Pacific Rise or the ridges and trenches and the S. Atlantic Ocean (being close to the fresh water reservoir of Antarctica) offer great potential of oceanic information with regard to the general problem of rare gases, including ^3He.

B. SIGNIFICANCE OF THE $\delta(^3He)$ AND $\Delta'(He)$ CORRELATION

As described in Chapter III, a linear correlation between $\delta(^3He)$ and $\Delta'(He)$ has been observed for Pacific waters. This relationship is represented by the equation (10):

$$\delta(^3He) = (5.60 \pm 2.39) + (1.97 \pm 0.38)\ \Delta'(He).$$

The results are shown in Fig. 15. Three distinct groups of data points clustering around the solid line can be recognized. The near-surface ($\lesssim$500 m) and bottom (>3000 m), mid-depth (500 - 3000 m) and the E. Pacific Rise deep water samples lie respectively near the lower, central and upper section of the graph.

The values of the intercept and slope of the equation (10) are affected severely by the scatter of the

SCAN data. Removal of either the 2493 m or 2573 m data (different stations) would affect the intercept to a great extent. When the data from the three expeditions were treated individually the NOVA values yielded the lowest intercept (~2.87%). The results strongly demonstrate the necessity of sampling at uniform and closely spaced depths at various locations. It is interesting to note the tight cluster of four samples (927, 940, 1011, and 1091 m) from four different stations (see central part of Fig. 15). Another group (from two locations only) lies in the lower section of the figure for the depth range of 3900 - 4300 m.

Even though the value of the intercept is $5.6 \pm 2.4\%$ -- contrary to the expected value of $\delta(He^3) = -1.4\%$, and $\Delta'(He^4) = 0$ for surface waters, the existence of a correlation in itself seems very significant. The correlation between the $\Delta'(He)$ and the $\delta(^3He)$ implies that the excess oceanic ^3He and ^4He have a common source -- the solid earth, since this is the only plausible source of excess radiogenic ^4He. The origin of ^3He will be discussed in a later section.

The intercept cannot be explained by assuming the $\delta(^3He)$ data (properly corrected for ^3H-contribution to

the surface waters) to be erroneous because it is just a ratio anomaly relative to the atmospheric $^3He/^4He$ ratio and is independent of any solubility data. As mentioned in Chapter III, the $\delta(^3He)$ values were determined by interspersing the sea samples with air samples of known size under identical experimental conditions. Therefore the reason that the intercept does not lie close to the origin might be caused by a systematic error in $\Delta'(He)$ values computed from equation (6), i.e., $\Delta'(He) = \Delta(He) - f[\Delta(Ne)]$; here f is dependent upon C^* and p of He and Ne (see equation 7), therefore errors in the variables C^* and p_o will affect the calculated values for $\Delta'(He)$. Various possibilities that could influence $\Delta'(He)$ are discussed below.

(i) Under equilibrium conditions at the sea surface the solubility of a gas is directly proportional to its partial pressure p in the gas phase, which in turn is equal to the ambient atmospheric pressure times the atmospheric concentration p_o of the gas. As far as the changes in the former are concerned, they affect the Δ values of He and Ne equally, thus leaving p_o as the only variable that could yield erroneous solubility data. However, it seems unlikely that the p_o values are (see

Table I) in error as they have been unchallenged in the literature for two decades. Nonetheless, such a possibility cannot be completely ruled out in view of the fact that the measurements have never been repeated. Since these measurements (21) were carried out by fractionation of He and Ne, an increase of 1.5% in the presently accepted Ne content of the atmosphere would mean an equal decrease in the He content. Hence $\Delta'(He)$ values would increase by 3%, which is about the right amount required to force the $\delta(He^3)$-$\Delta'(He)$ intercept through the origin.

(ii) If temperature variations occur after a certain water parcel has lost its contact with the atmosphere, $\Delta(Ne)$ is altered more than the $\Delta(He)$. Thus warming from 0° to 20° would lead to a decrease of 13 to 5% respectively for Ne and He solubilities. Now if such a situation existed, the $\Delta'(He)$ value would push the line (see Fig. 15) to the right. However in order to evaluate the fine structure of $\Delta(He)$ and $\Delta(Ne)$ due to such effects, measurements on the same samples for other rare gases are necessary.

(iii) The negative intercept of $\Delta'(He)$ can also be caused by the partial dissolution of air bubbles that are carried into the sea water. Any bubble in sea water is

at a total pressure of one atmosphere plus the prevailing hydrostatic pressure. Therefore its partial dissolution would enrich the waters by an amount lying between the original gas contents dissolved when it was at the sea surface and the contents produced by the complete dissolution of the bubbles. Bubbles of 100 - 1000 μ diameter are formed in the upper one meter of the sea and as they travel downwards, the partial pressure of the gases inside them increases 10% per meter. Under such conditions, diffusion of the gases into the surrounding water is determined by the product βD (20), where β is the Bunsen solubility coefficient and D is the diffusion coefficient of the gas in sea water.

Therefore the condition for enrichment of Ne relative to He in a bubble is given by $(\beta D)_{Ne} < (\beta D)_{He}$. The βD values quoted by Craig and Weiss (20) for He and Ne relative to Ar at 22°C are 0.82 and 0.59 respectively, thus demonstrating that the subsurface bubbles should be enriched in Ne with respect to He. Therefore the Δ(He) measured for these waters will always be slightly too low, and must be compensated by reducing the Δ(Ne) proportionately, i.e. f should be reduced from ~1.17 to get the correct Δ'(He).

Even though the precise data on the life times of the bubbles in sea water is not available, the $\delta(^3He)$-$\Delta'(He)$ correlation strongly suggests that the subsurface waters are enriched in Ne by the bubbles and therefore the resultant $\Delta'(He)$ data has been overcorrected. This is also substantiated by the negative $\Delta'(He)$ ($\sim$3%) values computed for the S. Atlantic Ocean (Fig. 13), where all the $\Delta(He)$ is due to air injection. Therefore the magnitude of overcorrection in $\Delta'(He)$ is approximately 3%, which would make the graph pass through the origin (see Fig. 15). This would also be an upper limit of the expected effect on $\Delta(He)$ due to partial dissolution of the air bubbles.

C. HELIUM ISOTOPE FLUXES

Estimates of the ^3He and ^4He fluxes from sea to atmosphere can be made using two models, the "Box-model" and "Diffusion-Advection model", described by Craig and Clarke (28). Both the models account for advection of bottom water upward through the deep water column (1-4 km). However, an additional term for eddy diffusion flux is built into the diffusion-advection model, thus yielding

a better estimate.

The ^3He flux (Φ_3) relationships based on these models are;

Box-model (advection only)

$$\Phi_3 \text{ (atoms cm}^{-2} \text{ sec}^{-1}) = 2.5\text{x}10^6 \ (\Delta_M' - \Delta_o')_3 \ W(\alpha R_A), \text{---(11)}$$

Diffusion-Advection model

$$\Phi_3(\text{atoms cm}^{-2} \text{ sec}^{-1}) = (2.5\text{x}10^6)W(\alpha R_A)\left[\frac{z^*}{z}(\Delta_{xt}'-\Delta_m')_3 + (\Delta_m'-\Delta_o')_3\right], \text{----------(12)}$$

where:

Δ_M' = Mean Δ' of the deep water profile.

$(\Delta_o')_3$ = $(\Delta_o')_4$, Original saturation anomaly of nascent bottom water at the sea surface.

W = Upward advective velocity through deep water mass = 5 m/yr (37).

R_A = Atmospheric ($^3He/^4He$) ratio = 1.4×10^{-6} (22).

α = Helium isotopic fractionation factor = 0.988 (18).

z^* = Ratio of the turbulent diffusion coefficient to the advective velocity = 1 km^{-1} in the Pacific (37).

Δ_{xt}' = Δ' value for maximum $\delta(^3He)$ in the deep water profile.

Δ_m' = Δ' value for $\delta(^3He)$ observed at the top of deep water mass.

Z = Depth variation (in km) for the above two $\delta(^3He)$ values.

The first and second terms of equation (12) represent the eddy diffusion and vertical advection flux respectively. For obtaining ^4He flux (Φ_4), the term (αR_A) is omitted and subscript 3 is replaced by 4 in equations (11) and (12). A value of $(\Delta'_o)_4 = -3.5\%$ is obtained from equation (10) by substituting $\delta(^3He) = -1.2\%$, the ^3He fractionation value at 0°C (18). Since equation (10) was deduced from the Pacific helium data (excluding the anomalous $\Delta'(He)$ data of SCAN Station 56), the ^3He and ^4He fluxes have been calculated for the same stations. For the NOVA station, the deep water mass starts at 866 m indicated by the salinity minimum, and the maximum ^3He value is observed at 1737 m (see Figs. 9 and 11). Because of this the ^3He concentration gradient is assumed to be represented by these two extremes, i.e., $(\Delta'_{xt})_3 = 31.5\%$ and $(\Delta'_m)_3 = 4.2\%$ (see Table VI). In the case of ^4He, even though the maximum occurs around 2.4 km with $\Delta'(He) = 8.7\%$ (Fig. 11), the figure of 6.7% corresponding to 1737 m is used so that Φ_3 and Φ_4 could be evaluated using the same depth interval from the Diffusion-Advection model. A similar procedure was adopted for cumulative SCAN data (except station 56), where the deep water mass

starts around 940 m (32), thus extreme $\delta(^3He)$ values were chosen at 940 m and 2493 m (Table IX) depths.

As far as the calculation of ^3He fluxes at the GEOSECS location is concerned, the T-S diagram (Fig. 9) shows a well-mixed water mass starting at 208 m and extending all the way to the bottom. The upper boundary is therefore taken at 208 m whereas the $(\Delta'_{xt})_3$ corresponds to maximum $\delta(^3He)$ observed at 1955 m (Table VII). A $\delta(^3He)$ value of 3% -- extrapolated from the $\delta(^3He)$ versus depth curve (Fig. 12), was used to obtain $(\Delta'_m)_3$ since the oceanic gradient is altered by artifical tritium at this location (17,27).

The flux estimates from both the models along with other pertinent data are given in Table XI. It can be seen from the Diffusion-Advection calculations that:

$$\Phi(\text{E.P.R.}) \sim \Phi(\text{S.Pacific}) > \Phi(\text{N. Pacific})$$

for either isotope. The average ^3He and ^4He fluxes of non-atmospheric origin for the three locations are:

$$\bar{\Phi}_3 = 5.9 \pm 1.8 \text{ atoms cm}^{-2} \text{ sec}^{-1}$$

$$\bar{\Phi}_4 = (1.2 \pm .2) \times 10^6 \text{ atoms cm}^{-2} \text{ sec}^{-1};$$

and yield a flux ratio, $\frac{\Phi_3}{\Phi_4} = 5 \times 10^{-6}$, which is 3.6 times the atmospheric helium ratio. It is noteworthy that the

TABLE XI. FLUX ESTIMATES OF OCEANIC HELIUM

STATION		Box-Model Calculations*			Diffusion-Advection Model Calculations*						
		Δ'_M ** ‰	Boundaries*** Used	Flux Φ atoms $cm^{-2} sec^{-1}$	Δ'_{xt} ‰	Δ'_m ‰	Extremes of Enriched Water	Z km	Flux Φ (atom cm^{-2} sec^{-1}) Diffusive	Advective	Total
NOVA (S. Pacific)	^3He	21.6	1000 to 3400 m	4.3	31.5	4.2	866 to 1737 m	0.87	5.4	1.3	6.7
	^4He	5.6		1.1×10^6	6.7	1.2			0.8×10^6	0.6×10^6	1.4×10^6
GEOSECS (N. Pacific)	^3He	25.5	>208 m	5.0	30.3	6.3	208 to 1955 m	1.75	2.4	1.7	4.1
	^4He	5.4		1.1×10^6	5.6	2.0			0.3×10^6	0.7×10^6	1.0×10^6
SCAN (E. Pacific Rise)	^3He	36.1	>900 m	6.9	43.0	23.8	940 to 2493 m	1.55	2.1	4.7	6.8
	^4He	8.3		1.5×10^6	6.1	5.8			0.02×10^6	1.16×10^6	1.2×10^6
Average				$\Phi_3 = 5.4 \pm 1.5$****							$\Phi_3 = 5.9 \pm 1.8$
				$\Phi_4 = (1.2 \pm .2) \times 10^6$							$\Phi_4 = (1.2 \pm .2) \times 10^6$

* Δ'_o for both models is -3.5‰.

** $(\Delta'_m)_3$ obtained from averaged $\delta(^3He)$ and $\Delta'(He)$ values lying between the boundaries.

*** Based on T-S diagrams and $\delta(^3He)$ profiles.

**** Maximum deviation from the mean value. Equivalent to the resultant error if errors in individual Δ were used. A systematic error of 40% in W should also be included.

$\bar{\Phi}_4$ value compares reasonably well with the flux expected from the decay of radioactive elements (~2 x 10^6 atoms cm^{-2} sec^{-1}) described in Chapter I.

D. ORIGIN OF HELIUM-3

1. Terrestrial Helium

^4He is generated by the decay of uranium and thorium in the earth's crust; the influx into the atmosphere is approximately 2 x 10^6 atoms cm^{-2} sec^{-1}. The chief source of ^3He, on the other hand, is considered to be cosmic ray interactions in the upper atmosphere producing a flux of ~1.0 atom cm^{-2} sec^{-1}. Even though ^3He and ^4He are produced by different mechanisms, their residence times in the atmosphere are of the order of 10^6 years (38). Therefore a substantial loss of both ^4He and ^3He is necessary to explain the actual observed atmospheric content of these gases. The helium abundance in the atmosphere is 5.24 parts per million (21) with a $^3He/^4He$ ratio of 1.40 x 10^{-6} (22).

In previous estimates, the loss of helium from the earth's atmosphere was considered to be a thermal process occurring in the upper atmosphere (>120 km) (39). The

high temperature (~3000°K) at such altitudes can impart to a fraction of helium atoms velocity greater than their escape velocity. However, Nicolet (38) demonstrated that the thermal escape mechanism alone is unable to explain the observed atmospheric $^3He/^4He$ ratio due to following considerations. If the temperature of the thermopause (i.e., escape region) were high enough to cause the required loss of ^4He, then ^3He would be removed at a rate far in excess of its production. On the other hand, if ^3He escaped thermally and was in equilibrium, then ^4He would remain trapped. This implied the existence of some competing non-thermal process. The estimated average thermal loss rates are 5.9 and 6×10^4 atoms cm^{-2} sec^{-1} for ^3He (40) and ^{4}(He) (41) respectively; the latter falls short of the ^4He production rate by a factor of ~30. The ^3He thermal loss rate by contrast, is six times its assumed production rate thus pointing out the need for additional production mechanisms for ^3He.

Wasserburg et al. (42), MacDonald (41), Axford (43,44), Patterson (45), and Johnson and Axford (40) have studied this problem in recent years. They have re-examined the estimates of influx and loss rates of helium isotopes and suggested various non-thermal mechanisms for the loss of atmospheric helium. But, most of these

processes are inadequate because they are either unable to generate the required flux of ^4He (2×10^6 atoms cm^{-2} sec^{-1}) or they are unable to account for the ^3He balance in the atmosphere. However, the polar wind mechanism, recently suggested by Axford (43), appears to provide a satifactory solution to the ^4He problem. This process assumes that every helium ion produced by photo-ionization by solar ultraviolet at altitudes >400 km and geomagnetic latitudes $\gtrsim 60^\circ$ ultimately escapes the earth's atmosphere via geomagnetic field lines. Axford calculated a non-thermal ^4He loss rate of 7.6×10^6 atoms cm^{-2} sec^{-1}, which is of the order of the ^4He production rate quoted earlier. The non-thermal removal of ^3He due to this process amounts to ~ 1.25 atoms cm^{-2} sec^{-1}, thus implying that the thermal escape of ^3He still dominates the non-thermal loss by roughly a factor of 5; the total ^3He loss rate is ~ 7 atoms cm^{-2} sec^{-1}.

The most recent estimates of production and loss rates of ^3He and ^4He through various mechanisms are presented in Table XII. It can be seen that even though the ^4He budget is accounted for, the problem of the ^3He budget is not completely resolved. The present oceanic $\delta(^3He)$ measurements, however, indicate a flux of 5.9 atoms

TABLE XII. INVENTORY OF ATMOSPHERIC HELIUM

PRODUCTION			LOSS		
Mechanism	Flux atoms cm^{-2} sec^{-1}	Reference	Mechanism	Flux atoms cm^{-2} sec^{-1}	Reference
HELIUM-4					
Radioactive Decay of U and Th	$(2 \pm 1) \times 10^6$	41,43	Thermal	$\sim 6 \times 10^4$	41
Auroral Precipitation of Solar Wind Plasma	$\sim 10^4$	44	Non-thermal (polar wind)	$(7.6 \pm 3.8) \times 10^6$	43
Total	$(2.0 \pm 1.0) \times 10^6$			$(7.7 \pm 3.8) \times 10^6$	
HELIUM-3					
Galactic Cosmic Ray Interactions producing ^3H and ^3He	$0.40 \pm .15$	40,46,47, 48,49,50	Thermal	5.9 ± 3.0	40
			Non-Thermal (polar-wind)	1.25 ± 0.63	40
			Total	7.2 ± 3.6	
Accretion of Galactic and Solar Cosmic Rays	≤ 0.02	40			
Solar Cosmic Ray Interactions	$\simeq 0.01$	48			
(n,α) Reactions in the Earth's Crust	$\simeq 0.10 \pm .05$	51			
Meteorites and Cosmic Dust	negligible	see the text			
Reversal of the Earth's Magnetic Field	negligible	see the text			
	$\sim 0.5 \pm .2$				
Auroral Precipitation of Solar Wind Plasma	4.0 ± 2.0	40			
Primordial ^3He	5.9 ± 1.8	cf. Table XI			
Total	10.4 ± 4.0				

cm^{-2} sec^{-1}. Thus there appears to be an additional source of ^{3}He, presumed to be of primordial origin (16). There are various possible mechanisms for ^{3}He production apart from assuming a primordial origin. These alternate mechanisms are examined in the following sections.

2. (n,α) Reactions in the Lithosphere

(n,α) reactions have been proposed to be a source of ^{3}He production in the lithosphere. The neutrons required for inducing such reactions are generated by spontaneous fission of ^{238}U and an approximately equal number of neutrons arising from various (α,n) reactions on light elements (O, Al, Si) contained in the rocks. Out of all the possible (n,α) reactions, Morrison and Pine (51) show that the $^{6}Li(n,\alpha)^{3}H \xrightarrow{\beta^-} {}^{3}He$ is the most favoured reaction for producing ^{3}He. Contribution of ^{3}He from other nuclear reactions is either far less than this reaction or ruled out by energy considerations.

Assuming equal diffusion rates for helium isotopes, they (51) have developed the following relationship for computing the $^{3}He/^{4}He$ ratios in rocks of different types;

$$^{3}He/^{4}He = \varepsilon(\alpha,n)P_{th}(N\sigma)_{Li} \Big/ \sum_{Z}(N.\sigma)_{Z},$$

where $\varepsilon(\alpha,n)$ is the number of neutrons per α-particle formed in the rocks; P_{th}, the probability of reaction with a thermal neutron; N, the number of atoms of Li (or element Z) per gram of rock; and σ, the thermal neutron capture cross section of the same element. It can be shown that the $^3He/^4He$ ratio is decreased not only by increase in the concentration of U and Th, but also by decrease in the content of Li and by decrease in the content of the light elements Al, O, Si, the principal targets of the (α,n) reactions. With the present concentration of the elements in the earth's crust, the computed ($^3He/^4He$) ratio agrees with the experimental data (52,53,54).

On the basis of this theory, the expected ^3He production rate for the earth's crust is 0.10 atom cm^{-2} sec^{-1} with $^3He/^4He$ ratio of $\sim 1 \times 10^{-7}$ (51). Therefore in order to produce the oceanic ^3He flux = 5.9 atoms cm^{-2} sec^{-1}, a Li content about 60 times higher should be present in the oceanic crust or mantle, which is clearly impossible. Thus, nuclear processes in the lithosphere cannot be a possible source of the observed ^3He in the oceans.

3. Cosmic Dust

Cosmic dust is the meteoritic dust collected by the atmosphere from the space and from disintegration of meteorites passing through the atmosphere. However, the flux of this material is so small ($\lesssim 10^{11}$ g yr^{-1}) over the surface of the earth (55) that it can only be found in sediments or polar ice that accumulates very slowly. Cosmic ray spallation (56) and solar wind irradiation (57) of the cosmic dust is a possible source of ^3He, ^3H, and ^4He in the atmosphere. Therefore, the dust that settles through the ocean water could have helium contents as high as that of the meteorites ($^3He/^4He \sim 10^{-1}$-10^{-4} with $^3He \sim 10^{-7}$ cm^3 gm^{-1} (58,59). An influx of 10^{11} g yr^{-1} of extraterrestrial material having a meteoritic ^3He content would yield a value of $\sim 2 \times 10^{-3}$ atoms cm^{-2} sec^{-1} for ^3He flux. This is about 3000 times less than the observed oceanic ^3He flux.

Also, in order to explain the observed mid-depth maximum by means of cosmic dust, one would have to suppose that the dust dissolved and released its ^3He at just the right rate to produce the mid-depth maximum. However, one would then expect to find similar profiles in the Atlantic and Pacific oceans, and that the excess ^3He

would not be correlated with the excess Δ'(He) except by coincidence. The observed data do not seem to support the view that cosmic dust is responsible for the excess ^{3}He both from the point of view of the known influx of extraterrestrial material, the observed profiles in the Pacific and Atlantic, and the correlation between $\delta(^3\text{He})$ and Δ'(He).

4. Auroral Precipitation of Solar Wind

Johnson and Axford (40) have suggested that about 4.0 atoms cm^{-2} sec^{-1} of ^{3}He are being captured by the earth's atmosphere from the solar wind as it flows past the magnetosphere of the earth. This process, based on the deep penetration of the atmosphere by auroral primary ions of solar wind origin without immediate loss into space, yields a production rate that is five times the production rate from all sources except the primordial mechanism, and comparable to the latter. However, even if such a high value, which needs substantiation, of ^{3}He influx is assumed, it cannot explain the $\delta(^3\text{He})$ profiles -- the mid-depth maximum feature. Since auroral precipitation of the solar wind would occur mainly in high latitudes, the maximum $\delta(^3\text{He})$ values would be

expected in high latitude and bottom waters, as the latter are formed by sinking high latitude surface waters.

5. Reversal of the Earth's Magnetic Field

The reversal of the earth's magnetic field with time has been established from magnetic polarity determinations of volcanic materials. During a polarity transition, the earth's field is 10 - 30% as intense as in normal times (60,61), thus the earth loses some of its magnetic shielding against cosmic rays, which could presumably lead to high ^{3}He influx. Although some workers (62) have reported evidence of faunal extinctions coincident with geomagnetic reversals in sedimentary cores, it has been pointed out by Harrison (63) that one would not expect striking changes in mutation rates to occur in deep sea fauna, which are protected from cosmic radiation by the depth of the sea water. He estimates that during a reversal, organisms at the equator would receive ~14% more cosmic radiation than they do at present. Any significant enhancement of cosmic radiation at sea level has also been questioned by others (64).

In spite of all the above arguments, even if a high ^3He flux did occur during the last reversal that took place 2 x 10^4 years ago (65) because the oceanic mixing time is only about 10^3 years, it would seem impossible for a memory of the last reversal to still be imprinted in the oceans at the present time.

6. Primordial Helium-3

In summary, the various ^3He sources discussed above and tabulated in Table XII, seem unable to generate the ^3He flux observed for ocean waters or to balance the total loss rate of ^3He from the atmosphere. The major difficulty lies in explaining the mid-depth $\delta(^3He)$ maximum, the near-zero $\delta(^3He)$ values for the ocean surface and intermediate values in the bottom waters -- a general feature of the oceanic data. On the other hand, all these observations can be easily justified if a source within the oceans is postulated. The present data further substantiates the primordial origin of ^3He (16), that is, the ^3He contribution to higher $^3He/^4He$ ratios found in the ocean waters are assumed to be due to a fraction of primordial ^3He incorporated into the earth at the time of its formation.

The flux estimates on the basis of present data average to 5.9 atoms cm^{-2} sec^{-1}, which is higher than the flux contribution from any other source (cf. Table XII). It is also noteworthy that the primordial ^3He flux alone equals the ^3He thermal loss rate, which seems to suggest that only these two processes are necessary to control the atmospheric abundance of ^3He.

These results for the average $^3He/^4He$ flux ratio of non-atmospheric origin i.e., 5×10^{-6} (Section C) are in good agreement with a value of $\sim 10^{-5}$ reported for volcanic gases (54) from the southern Kurile Islands (~46°N, 149°E); volcanoes being the most obvious outlet of primordial gases from the interior of the earth.

Following the procedures outlined earlier (16), the oceanic ^3He flux yields a limiting value of $\sim 3 \times 10^{-11}$ cm^3 STP/g for the original content of ^3He in the earth 5×10^9 years ago, assuming a constant degassing rate. The gas-rich meteorites, a special class of stone meteorites with 10% abundance, exhibit $^3He/^4He$ and ^3He content values of about 3×10^{-4} and 10^{-7} cm^3 STP/g respectively (59) -- these high values are attributed to the primordial helium gas in meteorites. Thus an average ^3He content of 10^{-8} cm^3 STP/g is obtained for all

meteorites, which is about 300 times the original ^3He content of the earth as estimated from oceanic ^3He data. The ^3He degassing rate during the early history of the earth might have been much higher than the present-day rate. Therefore, the original ^3He content of the earth could very well have been as high as the value found for stone meteorites ($\sim 10^{-8}$ cm^3 STP/g) in its early history. Thus, although the primordial origin of excess ^3He may not be susceptible to direct proof, no other mechanism examined so far seems capable of producing the observed flux.

If it is assumed that all the ^3He excess measured in subsurface waters is due to a primordial source with ^3He content equal to the mean meteoritic content, then it is concluded that there is $\lesssim 2\%$ primordial contribution to $\Delta'(He)$ -- the rest, ~98% being radiogenic. That is,

$$\left[\frac{\text{Non-atmospheric } (^3He/^4He)}{\text{Meteoritic } (^3He/^4He)}\right] \times 100 = \frac{5\times10^{-6}}{3\times10^{-4}} \times 100 \sim 2\%.$$

The proportion of primordial and radiogenic contributions to $\Delta'(He)$ does not seem unreasonable.

To conclude, the present investigations have achieved the following:

(i) ^3He, ^4He and Ne concentrations have been measured in ocean water -- ^3He for the first time.

(ii) The Pacific $\delta(^3He)$ values are roughly four times the Atlantic values -- with the highest values of $\lesssim$33.5% over the E. Pacific Rise locations.

(iii) Assuming all the Δ(Ne) to be of atmospheric origin, ~60% of the Pacific and all the Atlantic Δ(He) is explained as due to atmospheric injection.

(iv) The $\delta(^3He)$ depth profiles and subsequent flux estimates can be explained if a primordial source is postulated.

(v) A correlation between the $\delta(^3He)$ and Δ'(He) has been observed. Since the only possible source of radiogenic ^4He is the solid earth, this seems to prove that the ^3He excess is also from the same source.

APPENDIX A

DERIVATION OF $\Delta(^3He)$ RELATIONSHIP

By definition, the saturation anomalies for ^4He and ^3He and the ratio differences for ^3He can be written as:

$$\Delta_4(\%) = [(C_4/C_4^*)-1]100, \quad \text{- - - - - - - - - - - - - (i)}$$

$$\Delta_3(\%) = [(C_3/C_3^*)-1]100, \quad \text{- - - - - - - - - - - - - (ii)}$$

and

$$\delta_3(\%) = \left[\left(\frac{C_3}{C_4}\right)\Big/\left(\frac{p_{o(3)}}{p_{o(4)}}\right) - 1\right] 100, \quad \text{- - - - - - - (iii)}$$

where $\Delta_4 \equiv \Delta(^4He)$, $\Delta_3 \equiv \Delta(^3He)$, $\delta_3 \equiv \delta(^3He)$,

$C_i \equiv C(^iHe)$ = concentration of the i isotope in sea water in ml/kg,

$C_i^* = C^*(^iHe)$ = Solubility of the i isotope in ml/kg,

and $p_o(i)$ = concentration of the i isotope in air. The solubilities of ^3He and ^4He are also related as:

$$\frac{C_3^*}{C_4^*} = \alpha\left[\frac{p_{o(3)}}{p_{o(4)}}\right], \quad \text{- - - - - - - - - - - - - - - - (iv)}$$

where α is the isotopic fractionation factor (18). Rearrangement of equations (ii) and (iii) yields:

$$C_3^*/C_3 = 100/(\Delta_3 + 100), \quad \text{- - - - - - - - - - - - - (v)}$$

and

$$\frac{p_o(3)}{p_o(4)} = \frac{(C_3/C_4)100}{\delta_3 + 100}, \quad \text{- - - - - - - - - - - - - - - (vi)}$$

respectively.

Substituting the $p_o(3)/p_o(4)$ ratio from equation (iv) into equation (vi), and rearranging, we get

$$\frac{C_3^*}{C_3} = \frac{\alpha\left[\frac{C_4^*}{C_4}\right]100}{\delta_3 + 100} \cdot \text{- - - - - - - - - - - - - - - - - - - (vii)}$$

But $(C_4^*/C_4) = \left[\frac{\Delta_4}{100} + 1\right]^{-1}$ according to equation (i).

Therefore equation (vii) becomes:

$$\frac{C_3^*}{C_3} = \frac{\alpha\left[\frac{\Delta_4}{100} + 1\right]^{-1} 100}{\delta_3 + 100}$$

and when equated with equation (v), the result is

$$\frac{100}{\Delta_3 + 100} = \frac{\alpha\left[\frac{\Delta_4}{100} + 1\right]^{-1} 100}{\delta_3 + 100} .$$

Rearrangement reduces this equation to:

$$\Delta_3 = \left(\frac{\delta_3 + 100}{\alpha}\right)\left(\frac{\Delta_4}{100} + 1\right) - 100,$$

which upon simplification renders the equation (9) mentioned

in Chapter III, i.e.,

$$\Delta_3(\%) = [\delta_3 + \Delta_4 + 10^{-2}\delta_3\Delta_4 - 10^2(\alpha-1)]\alpha^{-1}.$$

BIBLIOGRAPHY

1. Buch, K., J. Cons. int. Explor. Mer. 4 (1929) 162.
2. Rakestraw, N. W. and Emmel, V. M., J. Phys. Chem. 42 (1938) 1211.
3. Weiss, R. F., Deep-Sea Res. 17 (1970) 721.
4. Weiss, R. F., J. Chem. Engg. Data 16 (1971) 235.
5. Bien, G., Rakestraw, N. and Suess, H.; In "Radioactive Dating" (IAEA, Vienna - 1963) p. 159.
6. König, H., Wänke, H., Bien, G. S., Rakestraw, N. W. and Suess, H. E., Deep-Sea Res. 11 (1964) 243.
7. Revelle, R., and Suess, H. E.; In "The Sea" (M. N. Hill, ed.) Vol. I, (Interscience, New York - 1962) p. 314.
8. Paneth, F. A. and Peters, K., Z. Phys. Chem. 134 (1928) 353.
9. König, H., Z. Naturf. 18a (1963) 363.
10. Suess, H. E. and Wänke, H., Prog. Oceanog. 3 (1965) 347.
11. Mazor, E., Wasserburg, G. J. and Craig, H., Deep-Sea Res. 11 (1964) 929.
12. Bieri, R. H., Koide, M. and Goldberg, E. D., Science 146 (1964) 1035.

13. Bieri, R. H., Koide, M. and Goldberg, E. D., J. Geophys. Res. 71 (1966) 5243.

14. Craig, H., Weiss, R. F. and Clarke, W. B., ibid. 72 (1967) 6165.

15. Bieri, R. H., Koide, M. and Goldberg, E. D., Earth Planet. Sci. Letters 4 (1968) 329.

16. Clarke, W. B., Beg, M. A. and Craig, H., ibid. 6 (1969) 213.

17. Clarke, W. B., Beg, M. A. and Craig, H., J. Geophys. Res. 75 (1970) 7676.

18. Weiss, R. F., Science 168 (1970) 247.

19. Benson, B. B. and Parker, P. D. M., Deep-Sea Res. 7 (1961) 237.

20. Craig, H. and Weiss, R. F., Earth Planet. Sci. Letters 10 (1971) 289.

21. Glueckauf, E., In "Compendium of Meteorology" (Amer. Meteorological Soc., Boston - 1951) p. 3.

22. Mamyrin, B. A., Anufrier, G. S., Kamensky, I. L. and Tolstikhin, I. N., Geokhimiya No. 6 (1970) 721.

23. Weiss, R. F., Deep-Sea Res. 15 (1968) 695.

24. Norton, F. J., In "Trans. AVS Nat. Vac. Symp., 1961" (Pergamon Press, Oxford - 1962) p. 8.

25. Eberhardt, P., Eugster, O., and Marti, K., Z. Naturf. 20A (1965) 623.

26. Craig, H. and Weiss, R. F., J. Geophys. Res. 75 (1970) 7641.

27. Roether, W., Münnich, K. O. and Östlund, H. G., ibid. 75 (1970) 7672.

28. Craig, H. and Clarke, W. B., Earth Planet. Sci. Letters 9 (1970) 45.

29. York, D., Can. J. Phys. 44 (1966) 1079.

30. Dockins, K. O., Bainbridge, A. E., Houterman, J. C. and Suess, H. E., In "Radioactive Dating and Methods of Low-Level Counting" (IAEA, Vienna - 1967) p. 121.

31. Warren, B. A., In "Scientific Exploration of the South Pacific" (W. N. Wooster ed. - National Academy of Sciences - Washington, D.C. - 1970) p. 33.

32. Sverdrup, H. U., Johnson, M. W. and Fleming, R. H. "The Oceans: their Physics, Chemistry and General Biology" (Prentice-Hall, New York - 1942) Chap. XV.

33. Wüst, G., Wiss. Ergebn. dtsch. Atlant. Exped. Meteor, 1925-27, 6 (1936) 1.

34. Broecker, W. S. and Olson, E. A., Science 132 (1960) 712; Broecker, W. S., In "The Sea" (M. N. Hill, ed.) Vol. II, (Interscience, New York - 1963) p. 88.

35. Von Herzen, R., Nature, 183 (1959) 882.

36. Bullard, E. C., In "The Sea" (M. N. Hill, ed.) Vol. III (Interscience, New York - 1963) p. 218.

37. Craig, H., J. Geophys. Res. 74 (1969) 5491.

38. Nicolet, M., Ann. Geophys. 13 (1957) 1.

39. Spitzer, L. Jr., In "The Atmosphere of the Earth and Planets" (G. P. Kuipor, ed.) 2nd Ed. (University of Chicago Press - 1952) Chap. VII.

40. Johnson, H. E. and Axford, W. I., J. Geophys. Res. 74 (1969) 2433.

41. MacDonald, G. J. F., Rev. Geophys. 1 (1963) 305.

42. Wasserburg, G. J., Mazor, E. and Zartman, R. E., In "Earth Sciences and Meteorites" (J. Geiss and E. D. Goldberg eds.) F. Houterman's volume (North-Holland, Amsterdam - 1963) p. 219.

43. Axford, W. I., J. Geophys. Res. 73 (1968) 6855.

44. Axford, W. I., In "Atmospheric Emissions" (B. M. McCormac and A. Omholt eds. - Van Nostrand Reinhold Co., New York - 1969) p. 317.

45. Patterson, T. N. L., Rev. Geophys. 6 (1968) 553.

46. Fireman, E., Phys. Rev. 91 (1953) 922.

47. Lal, D., and Peters, B., Prog. Elementary Particle and Cosmic Ray Physics 6 (1962) 3.

48. Nir, A., Kruger, S. T., Lingenfelter, R. E. and Flamm, E. J., Rev. Geophys. 4 (1966) 441.

49. Craig, H. and Lal, D., Tellus 13 (1961) 85.

50. Teegarden, B. J., J. Geophys. Res. 72 (1967) 4863.

51. Morrison, P. and Pine, J., Ann. N. Y. Acad. Sci. 62 (1955) 69.

52. Aldrich, L. T. and Nier, A. O., Phys. Rev. 74 (1948) 1590.

53. Khlopin, V. G., Doklady Akad. Nauk SSSR. 61 (1948) 297.

54. Mamyrin, B. A., Tolstikhin, I. N., Anufriyev, G. S. and Kamenskiy, I. L., Geokhimiya, No. 5 (1969) 595.

55. Parkin, D. W. and Tilles, D., Science 159 (1968) 936.

56. Signer, P. and Suess, H. E., In "Earth Sciences and Meteorites" (J. Geiss and E. D. Goldberg eds.) F. Houterman's volume (North-Holland, Amsterdam - 1963) p. 241.

57. Eberhardt. P., Eugster, O. and Geiss, J., J. Geophys. Res. 70 (1965) 4427; Wänke, H. Z. Naturf. 20A (1965) 946.

58. Honda, M., and Arnold, J. R., In "Handbuch der Physik, 46/2" (S. Flügge ed. - Springer-Verlag, Berlin - 1967) p. 613.

59. Pepin, R. O., and Signer, P., Science 149 (1965) 253.

60. Cox. A., Dalrymple, G. B. and Doell, R. R., Sci. Am. 216 (1967) 44.

61. Heye, D., Earth Planet. Sci. Letters 9 (1970) 82.

62. Opdyke, N. D., Glass, B., Hays, J. D. and Foster, J. H., Science 154 (1966) 349; Watkins, N. D., and Goodell, H. G., ibid. 156 (1967) 1083.

63. Harrison, C. G. A., Nature 217 (1968) 46.

64. Waddington, C. J., Science 158 (1967) 913; Black, D. I., Earth Planet. Sci. Letters 3 (1967) 225.

65. Stacey, F. D., "Physics of the Earth" (John Wiley and Sons, Inc., New York - 1969) p. 176.